The reaction mechanism of iron and manganese superoxide dismutases studied by theoretical calculations

Rulisek, Lubomir; Jensen, Kasper; Lundgren, Kristoffer; Ryde, Ulf

Published in:
Journal of Computational Chemistry

DOI:
10.1002/jcc.20450

2006

Document Version:
Peer reviewed version (aka post-print)

The reaction mechanism of iron and manganese superoxide dismutases studied by theoretical calculations

Lubomír Rulíšek[a], Kasper P. Jensen[b], Kristoffer Lundgren[b], Ulf Ryde[b]*

[a]Department of Molecular Modelling, Institute of Organic Chemistry and Biochemistry, Academy of Sciences of the Czech Republic, Flemingovo nam. 2, 166 10, Praha 6, Czech Republic

[b]Department of Theoretical Chemistry, Chemical Centre, PO Box 124, Lund University, S 221 00, Lund, Sweden.

*Corresponding author. Tel.: +46 - 46 222 45 02; Fax: +46 – 46 222 45 43

E-mail: Ulf.Ryde@teokem.lu.se

2006-01-10

We have studied the detailed reaction mechanism of iron and manganese superoxide dismutase with density functional calculations on realistic active-site models, with large basis sets and including solvation, zero-point, and thermal effects. The results indicate that the conversion of O_2^- to O_2 follows an associative mechanism, with O_2^- directly binding to the metal, followed by the protonation of the metal-bound hydroxide ion, and the dissociation of $^3O_2$. All these reaction steps are exergonic. Likewise, we suggest that the conversion of O_2^- to H_2O_2 follows an at least partly second-sphere pathway. There are small differences in the preferred oxidation and spin states, as well as in the geometries, of Fe and Mn, but these differences have little influence on the energetics and therefore on the reaction mechanism of the two types of superoxide dismutases. For example, the two metals have very similar reduction potentials in the active-site models, although they differ by 0.7 V in water solution. The reaction mechanisms and spin states seem to have been designed to avoid spin conversions or to facilitate them by employing nearly degenerate spin states.

1. Introduction

Superoxide dismutases (SOD)[1] are oxidative-stress induced enzymes, found in all aerobic organisms. There are at least three unrelated families of SODs with different folds. These are the structurally homologous[2] mononuclear iron or manganese containing SODs (FeSOD, MnSOD),[3,4] the binuclear copper–zinc SODs (CuZnSOD),[5] and the mononuclear nickel SOD.[6,7,8] These enzymes all catalyse the same reaction, disproportionation of the superoxide radical anion (O_2^-) to dioxygen and hydrogen peroxide:

$$2\ O_2^- + 2\ H^+ \rightarrow O_2 + H_2O_2 \qquad (1)$$

They prevent oxidative damage by radicals derived from water-induced superoxide dismutation, such as the very reactive $OH^{\bullet}$ radical or possibly singlet dioxygen[9], in aerobic organisms.[10] These unwanted reactions are very fast even uncatalysed, ~10^7 $M^{-1}s^{-1}$.[9] The purpose of the SODs is to convert O_2^- into less reactive H_2O_2 and O_2 before these side reactions take place (H_2O_2 can subsequently be disproportionated to O_2 and H_2O by catalases).

The various SODs differ in terms of specific function. CuZnSODs are found in eukaryotic cytoplasm[11] and are probably important for the clean-up of oxidative pollution from the radical-warfare of the immune system.[5] FeSODs are found in the periplasmic space of bacteria and in chloroplasts of plants, a few protists, and possibly in other eukaryotes,[3,12] providing resistance to environmental or immunological oxidative stress.[13] MnSODs are found in bacteria and in the mitochondria of eukaryotes, where most of the O_2 is reduced.[14] They are believed to protect DNA from endogenous oxidative stress. Interestingly, both FeSOD and MnSOD are better than the other at protecting their respective local environments.[15]

In the case of MnSOD and FeSOD, the mechanism of O_2^- dismutation involves

the metal ion (M) cycling between the III and II oxidation states:[16]

$$M^{III}SOD + O_2^- \rightarrow M^{II}SOD + O_2 \quad (2)$$

$$M^{II}SOD + O_2^- + 2\,H^+ \rightarrow M^{III}SOD + H_2O_2 \quad (3)$$

The details of this mechanism is of utmost biochemical importance as it is involved in most oxidative-stress induced disorders. Many diseases, among those cancer and amylotrophic lateral sclerosis (ALS), can be caused by the radical damage of biological molecules, and the interest in therapeutic mimics is growing.[17,18,19] The reaction is also appealing owing to its speed; SODs work at rates close to the diffusion limit, e.g. $k_{cat}/K_m \approx 2{\cdot}10^9\ M^{-1}s^{-1}$ for human MnSOD.[20] Moreover, there is a growing interest in understanding the differences between the Fe and MnSODs in terms of function and biological evolution.[3,21]

Recently, atomic resolution (0.9 Å) crystal structures of Mn^{II} and Mn^{III}SODs have been presented.[22] Although these are in fact mutants (Tyr174Phe), the structures are currently the best available for MnSOD. For FeSOD, crystal structures of a resolution down to 1.8 Å (Fe^{II})[23] and 1.6 Å (Fe^{III})[24] are available. The active sites in the resting state contain a five-coordinate distorted trigonal bipyramid metal and include three histidine (His) residues (one axial and two equatorial) binding via their $N^{\varepsilon 2}$ atoms to the metal ion. The two remaining coordination sites are occupied by an aspartate residue (Asp) in the equatorial position and a solvent molecule in the other axial position. The consensus is that this molecule is a hydroxide ion in the oxidised sites, but a water molecule in the reduced sites.[3,25,26] Obviously, the details of protonation (the active site pK_as) are crucial to understand the mechanism by which these clusters oxidise and reduce superoxide radicals. The present view is that one proton comes from the coordinated water molecule, which is deprotonated during

metal oxidation.[3] The other proton comes from the solvent, via a proton-transfer pathway involving at least a glutamine and a tyrosine residue, which are strictly conserved (Gln-69/146 and Tyr-34 in Escherichia coli Fe/MnSOD).[3,27,28,29,30,31] Consequently, the two half reactions in Eqns. (2–3) can be modified to include the metal-bound solvent molecule:

$$M^{III}SOD_{OH} + O_2^- + H^+ \rightarrow M^{II}SOD_{H_2O} + O_2 \quad (4)$$

$$M^{II}SOD_{H_2O} + O_2^- + H^+ \rightarrow M^{III}SOD_{OH} + H_2O_2 \quad (5)$$

Superoxide can in principle bind to the active site of SOD in three different ways: by replacing one of the normal ligands, most likely the solvent molecule (dissociative mechanism), by increasing the coordination number to six (associative mechanism), or without forming a direct bond to the metal ion (second-sphere mechanism). A six-coordinate, octahedral intermediate has been observed in both Fe^{III}SOD and Mn^{III}SOD crystal structures with N_3^-.[32] Likewise, spectroscopic studies indicate that the NO adduct to Fe^{II}SOD is six-coordinate.[33] Therefore, associative mechanisms are normally preferred. However, anions like N_3^- and F^- do not bind directly to reduced Fe^{II}SOD (but most likely to Mn^{II}SOD[34]), which has been interpreted in favour of a second-sphere binding of the substrate in this oxidation state.[3,35,36,37] A putative second-sphere binding site has been identified 7.5 Å from the metal ion, interacting with the conserved Tyr-34 and His-30 residues.[3,36] Moreover, spectroscopic studies of N_3^- and F^- bound to the oxidised enzymes have indicated that the metal looses one ligand at temperatures above 305 K,[38,39] although other investigations indicate that it is actually N_3^- or F^- that dissociates.[40] Finally, there is no guarantee that these substrate analogues behave the same way as the true O_2^- substrate.

Recently, theoretical studies of the mechanism of these key enzymes have

begun to emerge. McCammon and coworkers have studied the ionic-strength dependence of the rate constant of the association of superoxide to the protein.[41] Moreover, density functional theory has been used to supplement the rationalization of electronic structure and electronic absorption spectra.[42] Likewise, Brunold and coworkers have combined spectroscopic techniques with density functional theory and semiempirical calculations for the study of native, mutant, and metal-substituted Fe and MnSODs.[28,30,33,40,43,44,45] They have shown that second-sphere residues are involved in the substrate binding and selectivity, the tuning of the reduction potential and proton transfer in the active sites. Finally, Noodleman and coworkers have studied the reduction potentials of Fe and MnSOD and their coupling to the deprotonation of the metal-bound solvent molecule.[26,46,47] Again, the authors found important influence of second-sphere residues.

In this work we have performed a systematic computational study of possible intermediates expected to be involved in the reaction cycle of Fe- and MnSODs, concentrating on the intrinsic properties of the active metal sites and similarities and differences between the two metal ions. We have compared the various reaction mechanisms (associative, dissociative, or second-sphere) and evaluated thermodynamically possible pathways for both half-reactions, with a consideration of possible protonation states.

2. Methods

2.1 Computational details

All calculations have been carried out with the Turbomole 5.6 software.[48] The geometry optimisations were performed with the Becke-1988–Perdew-1986 (BP) density functional method. [49,50] The DZP basis set by Schäfer et al.[51,52] (14*s*11*p*6*d*1*f* /

8*s*7*p*4*d*1*f*) was used for the metals, whereas the 6-31G* basis set[53] was used for the other atoms. The calculations were sped up by expansion of the Coulomb interactions in auxiliary basis sets, the resolution-of-identity approximation.[54,55] Single-point energies were calculated for all the optimised geometries at the B3LYP/6-311+G (2d,2p) level of theory.[53,56] In these calculations, the metals were described by effective triple-ζ polarised basis sets, constructed by enhancing the DZP sets with additional *s*, *p*, *d*, and *f*-type functions (exponents for Fe: 0.01377232 (*s*), 0.134915 and 0.041843 (*p*), 0.1244 (*d*), and 2.5 and 0.8 (*f*); Mn exponents: 0.0128732, 0.04028, 0.12765, 0.1125, 2.25, and 0.8).

We applied the default (m3) grid size of Turbomole and made use of the default geometry convergence criteria, i.e. 10^{-6} Hartree (2.6 J/mole) for the change in energy and 10^{-3} a.u. for the maximum norm of the internal gradient (5.0 kJ/mole/Å) between the two last iterations. All calculations were done with the unrestricted Kohn–Sham formalism. The reported spin densities have been obtained by the means of Mulliken population analysis. Zero-point energies and thermal corrections to the Gibbs free energy (at 298 K and 1 atm pressure, using an ideal-gas approximation[57]) were calculated from a frequency calculation, obtained with the same method as for the geometry optimisations. The binding free energies of the various molecules to the metal sites were corrected by a constant of –32 kJ/mole, representing the difference in the estimated translational entropy for $H_{0-2}O_2$ from the Sackur–Tetrode equation and from more reliable estimates.[58]

B3LYP is generally recognised as one of the most accurate density functional method for energies.[59,60,61,62,63] The BP and B3LYP methods often give somewhat different results. This is accentuated for the spin-splitting energies, for which BP gives an appreciably larger stability of the low- and intermediate-spin states (typically

by ~60 and 30 kJ/mole, respectively). This leads to an intermediate-spin ground state for the $Fe^{III}(Im)_3(AcH)(OH/H_2O)]^{2+}$ complexes, whereas B3LYP gives a high-spin ground state, in agreement with experiments.[64] Likewise, B3LYP gives correct ground states for the $Fe^{II}–NO_2$ (intermediate-spin) and $Fe^{III}–N_3^-$ (high-spin) models of FeSOD, whereas BP gives erroneous states. Therefore, we will only discuss B3LYP energies in the following.

2.2 Solvation energies

Normal quantum chemical calculations are performed in vacuum, whereas the interesting reactions take place in water solution or in proteins. In order to correct for this discrepancy, we have calculated solvation energies for all complexes using the continuum conductor-like screening model (COSMO) model[65], as implemented in Turbomole 5.6.[66] In this method, the solute molecule forms a cavity within a dielectric continuum characterised by a dielectric constant, ε. The charge distribution of the solute polarises the dielectric medium and the response of the medium is described by the generation of screening charges on the surface of the cavity.

These calculations were performed with default values for all parameters (implying a water-like probe molecule) and with a dielectric constant of 4 and 80, to model both pure water and access possible effects in a protein (where the effective dielectric constant is normally estimated to 2–16[67,68]). For the generation of the cavity, a set of atomic radii has to be defined. We used the optimised COSMO radii in Turbomole (H: 1.30 Å, C: 2.00 Å, N: 1.83 Å, O: 1.72 Å, Fe and Mn 2.00 Å).[69]

Reduction potentials were estimated from these energies in a solvent according to:

$$E^0 = E(\text{ox}) - E(\text{red}) - 4.43 \text{ eV} \quad (6)$$

where the factor of 4.43 eV represents the potential of the standard hydrogen electrode[70].

2.3 Model complexes

This study is based on small quantum chemical models of the active site. All models include one acetate ion (Ac) and three imidazole (Im) molecules, as models of the Asp and His ligands. In addition, H_2O or OH^- as a model of the metal-bound solvent molecule could be included, as well as an O_2^--derived ligand (O_2, HO_2, or H_2O_2 with various formal charges). For both oxidation states of the metal (M^{II} or M^{III}), we have studied the four-coordinate $[M(Im)_3(Ac)]^{+/2+}$ model, five-coordinate models with H_2O or OH^-, and dissociative (five-coordinate), associative (six-coordinate), and second-sphere (five-coordinate) models with O_2, HO_2, and H_2O_2. Second sphere ligands are denoted by a "+" before the ligand, e.g. $M(Im)_3(Ac)(OH)+O_2$. Hydrogen peroxide complexes were only studied in the M^{III} state. For the other two substrate molecules, the following four formal oxidation states were considered: $M^{II}+O_2^-$, $M^{III}+O_2^- = M^{II}+O_2$, $M^{II}+HO_2 = M^{III}+HO_2^-$, and $M^{III}+H_2O_2$. Some examples are shown in Figure 1.

The description of the complexes is complicated by the possibility of internal proton transfer. For example, water in all complexes forms a hydrogen bond to the Asp ligand and in some cases, the shared proton is transferred to the Ac model, giving an AcH–OH tautomer (Figure 1a). In the $[Fe^{II}(Im)_3(Ac)(H_2O)]^+$ complex, it is 8 kJ/mole less stable than the Ac–HOH tautomer, but in the $[Fe^{III}(Im)_3(Ac)(H_2O)]^{2+}$ complex, it is actually 4 kJ/mole *more* stable. The corresponding values for Mn are 11 and 34 kJ/mole. It is a general and conspicuous difference between Fe and Mn that Mn^{III} has a appreciably higher propensity for the AcH–OH tautomer than Fe^{III}. For

most complexes, we have considered both forms, but only the most stable one is given in the tables. Likewise, proton transfer is possible between the H_2O/OH ligand and the substrate O_2/HO_2/H_2O_2, but in this case we have optimised both states, so that we can estimate the energy of proton transfer.

Even the relatively small models used in this investigation can have many different conformations. This is always a problem in a theoretical investigation. However, because our aim is to calculate relative energies (reaction energies) and compare the energies and geometries of the two metal ions, the important thing is only to ensure that all structures studied have the same conformation. Therefore, we first performed a major survey of most conceivable structures of the various states. Then, we selected the same type of structures for both metal ions, ensuring that they are as similar as possible to the protein structure and that they are connected throughout the reaction mechanisms. Only the results of the latter structures are presented. This means that we only discuss associative structures with the substrate molecule binding trans to the Ac ligand (e.g. Figures 1c and e) and second-sphere structures where the substrate molecule forms a hydrogen bond to the solvent molecule (e.g. Figures 1b and f; in three cases this was not possible, owing to internal proton transfer). In crystal structures of the SOD proteins, the Ac ligand always bind in a monodentate mode (with only one oxygen coordinated to the metal). However, in the dissociative complexes and a few second-sphere complexes where the hydroxide ion is a hydrogen donor to the substrate, the Ac ligand prefers to bind in a bidentate mode (Figure 1d).

In the Tables, the complexes are first ordered according to the oxidation state of the metal and the substrate: Fe^{II}, Fe^{III}, Fe^{III}–H_2O_2, Fe^{III}–O_2^- = Fe^{II}–O_2, Fe^{III}–HO_2, Fe^{II}–O_2^-, and Fe^{II}–HO_2 = Fe^{III}–HO_2^-. Within each type of complex, the dissociative

states come first, followed by the associative H_2O (or AcH–OH^-) and OH^- complexes, and finally the second-sphere H_2O (or AcH–OH^-) and OH^- complexes.

3. Results and Discussion

3.1. Spin states and electronic structure

We will start by studying the relative stability of the different spin states of the various complexes. For all complexes, we have optimised the geometries in all possible spin states, although only high-spin states have been observed experimentally for the resting states, because this assignment is not obvious, especially not for complexes involving O_2^--derived ligands. The results are collected in Tables 1 (Fe) and 2 (Mn).

3.1.1 Spin states of the Fe models

From Table 1, it can be seen that all iron models are most stable in the high-spin (HS) states. This ground state is in accordance with experiment.[64] For the $Fe(Im)_3(Ac)$ and $Fe(Im)_3(Ac)(H_2O/OH)$ complexes, the intermediate-spin (IS) and low-spin (LS) states are ~70 and ~110 kJ/mole higher in energy for Fe^{II}, but only ~20 and ~80 kJ/mole for the oxidised Fe^{III} complexes. The spin-splitting energies vary only slightly (~1 kJ/mole) when calculated in continuum solvent with $\varepsilon = 4$ or 80.

For complexes with substrate molecules, the spin-splitting energies vary more and in a few cases the IS state comes quite close in energy to the HS ground state. It should be noted that for the ferric complexes with the O_2^- and HO_2 radicals, four (instead of three) spin states are possible (with 0, 2, 4, or 6 unpaired electrons) and the HS state has six unpaired electrons (five on iron and one on the radical).

It is notable that also the six-coordinate FeSOD models have HS ground states. This is in contrast to haem chemistry, which in general exhibits LS states for six-coordinated complexes.[71] This suggests that the three imidazoles and the acetate ion constitute a weaker equatorial ligand field than the porphyrin ring, thus allowing for occupation of all *d*-orbitals even upon six-coordination.

3.1.2 Electronic structure of the Fe models

Next, we look at the electronic structure of the various complexes, using the spin density on the iron ion and the substrate molecules (O_2, HO_2, or H_2O_2), shown in Table 1. From the complexes without any substrate or with the closed-shell product H_2O_2, it can be seen that the spin on iron quite clearly determines the oxidation and spin state of the system: For Fe^{II}, the LS, IS, and HS states have a spin population of (±)0.01–0.07, 2.03–2.06, and 3.80–3.88 a.u., respectively, whereas the corresponding states for Fe^{III} have spins of 0.89–1.10, 2.71–3.04, 4.09–4.39 a.u., respectively. Thus, the spin populations are quite close to the expected number of unpaired spins, except for HS Fe^{III}, for which part of the spin is delocalised on all ligands. Moreover, the Fe^{III} complexes exhibit a larger variation in the spin density than the reduced complexes.

For complexes with O_2 and HO_2, similar spin densities are found on the metal, although the ranges for each oxidation and spin state widen somewhat (e.g. to 0–0.28 a.u. for LS Fe^{II}), but still with no overlap. In fact, there are some IS HO_2 complexes that are best described as Fe^{IV}–HO_2^-, e.g. $[Fe(Im)_3(Ac)(OH)(HO_2)]^+$. The identification of the states is helped by the spin on the substrate (O_2, HO_2, or H_2O_2).

In the following we will concentrate on the HS ground states. We start with the Fe^{III}–O_2^- complex, which is formally equivalent with Fe^{II}–O_2, representing the first half-reaction of FeSOD (Eqn. 4). In the dissociative and associative complexes, the

metal remains mainly in the Fe^{III} oxidation state, with a spin population of 4.10–4.20 a.u., although O_2^- also gets an increased spin population of 1.32–1.53 a.u., i.e. nearly half-way to the product state. All the other iron ligands also have significant spin populations of 0.06–0.09 a.u. However, in the second-sphere complexes, internal electron transfer occurs fully, yielding essentially triplet $^3O_2$ with a spin of 1.68–1.92 a.u. ferromagnetically coupled to HS Fe^{II} (with ~3.9 unpaired spins). Thus, we can conclude that the first half-reaction of SOD is facile, with intermediate spin populations upon direct binding of superoxide and the automatic formation of triplet oxygen as the complex starts to dissociate.

For the corresponding protonated complexes (i.e. HO_2 radical bound to Fe^{III}), all coordination states give clear HS Fe^{III} complexes (spin 4.23–4.36 a.u.) with radical HO_2 (spin 0.95–1.03 a.u.). Likewise, the Fe^{II}–O_2^- complexes are well described by the formal oxidation states: a HS Fe^{II} ion (with spin 3.76–3.92) coupled to a superoxide radical anion (0.85–1.00 a.u.).

If the latter complex is protonated, as is expected in the second half-reaction of FeSOD, we obtain the formal Fe^{II}–HO_2 state, which is equivalent with Fe^{III}–HO_2^-. From Table 1, it can be seen that the associative and dissociative complexes are essentially in the Fe^{III}–HO_2^- form, with 4.14–4.21 a.u. spin on iron and 0.36–0.39 a.u. spin on HO_2^-. The second sphere complexes are HS Fe^{II} (3.81-3.91 a.u.) coupled to protonated superoxide radical (spin 0.95–1.00 a.u.). Moreover, these complexes tend to reorganise to the product H_2O_2 complex, and no $[Fe(Im)_3(Ac)(H_2O)+(HO_2)]^+$ structure was found unless HO_2 was allowed to interact only with the Im ligands. Again, this suggests that the active site is well designed to automatically drive the second half-reaction (Eqn. 5) in the correct direction.

3.1.3 Electronic structure and spin-splitting energies for the Mn models

Next, we turn to the corresponding manganese models presented in Table 2 and perform a similar analysis. We will discuss both the electronic structure and the spin-splitting energies at the same time, because these two properties are closely related.

The Mn^{II} and Mn^{III} complexes without substrate (resting states) and the Mn^{III}–H_2O_2 product complex have very pure spin states. The Mn^{II} complexes in their LS, IS, and HS states have 1.02–1.15, 3.18–3.25, and 4.91–4.98 unpaired electrons, i.e. close to the expected number. Likewise, the Mn^{III} complexes have 0.00–0.10, 2.06–2.15, and 4.01–4.20 unpaired electrons. Thus, we see that the spin states are well defined and widely separated from each other. In particular, it is clear that the spin delocalisation is smaller in the manganese complexes than in the corresponding iron complexes, especially for the HS states. This has been observed before.[72]

Moreover, all these complexes are most stable in their HS states, with the LS and IS states more than 100 kJ/mole higher in energy. Again, this is in accordance with available experiments.[64] This gives us some confidence in the assignment of states of the other models, which do not have experimentally determined spin states.

For complexes with O_2 or HO_2, the interpretation of the states becomes more complicated. This is mainly because the maximum number of unpaired spins changes as the metal is oxidised by the substrate: Thus, Mn^{II}–O_2 in its HS has seven unpaired electrons (five on Mn and two on $^3O_2$), whereas the formally equivalent Mn^{III}–O_2^- state can only have five unpaired electrons (four on Mn^{III} and one on O_2^-). For the corresponding Fe complexes, the HS state of both resonance forms had six unpaired spins because the electron is taken from a doubly occupied orbital in Fe^{II}. Therefore, the complexes with seven unpaired electrons will necessarily be Mn^{II}–$^3O_2$. It turned out that this state always had $^3O_2$ in the second coordination sphere – no dissociative

or associative models of this state could be found (therefore these states are missing in Table 2).

On the other hand, the state with five unpaired electrons turned out to be HS Mn^{III}–O_2^- with 3.93–4.35 spin on Mn and 0.63–1.03 spins on O_2^-. Such an electronic state was found for all types of complexes (dissociative, associative, and second-sphere). Moreover, for the dissociative and associative models, the lowest energy was obtained for the IS state (with three unpaired electrons), which is best interpreted as Mn^{III}–O_2^-, even if the spins are higher than expected from the pure spin states without any substrate: 4.13–4.30 spins on Mn and –1.14 to –1.35 on O_2^-.

The Mn^{III}–HO_2 complex can also go through an internal electron transfer to form the Mn^{IV}–HO_2^- complex. Again, the two resonance forms have a different maximum number of unpaired spins, five for the former, but only three for the latter (Mn^{IV} has only three 3*d* electrons). The state with five unpaired electrons is always Mn^{III}–HO_2 with 4.02–4.13 spins on Mn and 0.99–1.01 spins on HO_2. It is the ground state of the two second-sphere HO_2 complexes. However, for the dissociative and associative model with water, the Mn^{IV}–HO_2^- state is 10–22 kJ/mole lower in energy. Thus, the predicted ground state of these models is Mn^{IV}–HO_2^-, in variance to what was observed for iron. This reflects the higher stability of the +IV oxidation state for Mn than for Fe.

The situation is similar for the Mn^{II}–O_2^- complexes. The second-sphere complexes are most stable in the HS Mn^{II}–O_2^- state. However, for the associative complexes, the HS Mn^{III}–O_2^{2-} state (with four unpaired electrons) comes close in energy, and in the dissociative complex, this state is actually the predicted ground state.

Finally, the Mn^{II}–HO_2 complex can have a maximum of six unpaired spins,

whereas the $Mn^{III}–HO_2^-$ resonance form can have only four unpaired spins. For the dissociative and associative complexes, the HS state of the $Mn^{III}–HO_2^-$ resonance form (with four unpaired spins) turns out to be the ground state. However, all the second-sphere complexes are of the $Mn^{II}–HO_2$ form.

In conclusion, all the iron complexes have a HS ground state, whereas for the manganese models, the IS state is more stable for the first-sphere complexes with a substrate (only the dissociative complex for $Mn^{II}–O_2^-$). Moreover, Mn has a differing oxidation state for the dissociative $Mn^{III}–O_2^{2-}$ complex and for the first-sphere $Mn^{IV}–HO_2^-$ complexes (the corresponding iron complexes are $Fe^{II}–O_2^-$ and $Fe^{III}–HO_2^-$). In the following sections, we will investigate if this has any functional significance.

3.2 Geometries of the ground states

3.2.1 Comparison with crystal structures

The metal–ligand bond lengths of the optimised ground states are shown in Tables 3 (Fe) and 4 (Mn). For the five-coordinate resting states without any substrate, protein crystal structures are available and those with the highest resolution[22,23,24] have been included in the two tables. It is instructive to compare the experimental and calculated results to obtain an estimate of the accuracy of the quantum chemical geometries.

The general coordination geometry of the optimised models is trigonal bipyramidal (Figure 1a), which is in agreement with experiments. Thus, the proteins do not strain the coordination geometry away from the ideal one (i.e. they do not enforce a trigonal structure as opposed to square pyramid or four-coordinated with a second-sphere histidine or water molecule).

Moreover, the metal–ligand distances are well reproduced in the calculations. The reduced MnSOD structure (which has the best resolution, 0.9 Å) has $Mn–O_{Sol}$

distances (to the solvent molecule) of 2.26 and 2.28 Å (there are two independent subunits in the crystal). This compares well with the 2.23 Å distance in the $[Mn^{II}(Im)_3(Ac)(H_2O)]^+$ complex, which clearly shows that the solvent molecule is protonated in the reduced state; $Mn–O_{Sol}$ is much shorter (1.98 Å) in the complex with a hydroxide ion. This conclusion is in accordance with the experimental consensus.[3,25,26] The $Mn–O_{Ac}$ distance to the Asp ligand is even better reproduced: it is 2.05 Å in both experiments and calculations. For the His ligands, the results are similar: the calculated bond lengths are systematically 0.04–0.06 Å longer than the experimental ones, nicely reproducing also the elongation of the axial bond, compared to the two equatorial ligands. Thus, the calculations reproduce the experimental metal–ligand bonds within 0.06 Å, which is in accordance with our previous experience with this method.[73,74,75]

We next turn to the crystal structure of the oxidised Mn^{III}SOD.[22] Interestingly, the $Mn–O_{Sol}$ distance in this structure, 2.12–2.16 Å does not resemble the distance in any calculated structure: It is 1.78 Å in the expected deprotonated $[Mn^{III}(Im)_3(Ac)(OH)]^+$ structure and it is much shorter (1.85 Å) also in the corresponding protonated structure, because it prefers the AcH–OH tautomer. Even the less stable $[Mn^{III}(Im)_3(Ac)(H_2O)]^{2+}$ tautomer gives a $Mn–O_{Sol}$ distance of 2.07 Å. The reason for this discrepancy is that the Mn^{III} structure is reduced by electrons released by the intense X-rays during data collection. This is a well-known and serious problem of crystal structures involving groups that can be reduced.[76] Thus, the crystal structure of Mn^{III}SOD most likely contains a mixture of Mn^{III} and (especially) Mn^{II} active sites,[77] which makes this structure less useful for the judgement of the performance of the theoretical method. This has been suggested before.[34,47]

With this in mind, we now turn to the structure of Fe^{II}SOD.[23] From Table 3, it

can be seen that the experimental and calculated (for $[Fe^{II}(Im)_3(Ac)(H_2O)]^+$) Fe–$N_{His}$ and Fe–O_{Ac} distances are in reasonable agreement (within 0.08 Å). However, for the Fe–O_{Sol} distance, the discrepancy is larger than expected, 2.06 compared to 2.21 Å. However, it should be remembered that the resolution of this structure is appreciably lower than for the MnSOD structures, 1.8 Å. At this resolution, the average accuracy is 0.1 Å in the coordinates and errors of up to 0.3 Å are frequently observed, especially for metal–solvent bond lengths.[78,79,80,81] Therefore, and also because of the high accuracy of the quantum chemical structures for Mn^{II}SOD and for other metal sites,[73,74,75] we strongly believe that the calculated structures can be trusted. This is confirmed by the data for Fe^{III}SOD,[48] which shows the expected mixture of the $[Fe^{II}(Im)_3(Ac)(H_2O)]^+$ and $[Fe^{III}(Im)_3(Ac)(OH)]^+$ sites.

3.2.2 Geometries of the models

From the optimised geometries in Tables 3 and 4, it is clear that the Fe^{II} complexes typically give ~0.07 Å shorter bond lengths than the corresponding Mn^{II} complexes, which reflects the 0.05-Å difference in their ionic radii.[82] On the other hand, the bond lengths of Mn^{III} are ~0.04 Å shorter than those of Fe^{III}, although the variation is larger. The latter is probably caused by the fact that HS Mn^{III} has one empty 3*d* orbital and therefore is Jahn–Teller active (i.e. in an octahedral geometry, the two axial ligands will have a longer bond length than the four equatorial ligands).

The M–N_{Im} bond lengths in the various complexes are 2.07–2.35 Å for Fe^{II}, 2.03–2.33 Å for Fe^{III}, 2.14–2.49 Å for Mn^{II}, 1.99–2.43 Å for Mn^{III}, and 1.99–2.05 Å for Mn^{IV}, in accordance with the above concepts and also showing that that the bond lengths decrease when the formal charge on the metal increases. These bond lengths also decrease when the coordination number of the complex decreases. The M–O_{Ac}

bonds exhibit similar trends. The Fe–OH bonds are 1.85–1.99 Å, whereas the Mn–OH bonds are 1.78–1.90 Å for Mn^{III} and Mn^{IV}, but as much as 1.95–2.05 Å for Mn^{II}. The corresponding bonds to water are 2.04–2.21 Å for Fe and 2.06–2.23 Å for Mn.

However, it is the bonds to the substrate that exhibit the largest and most interesting variations. The $M^{III}–O_2H^-$ bond is ~0.07 Å shorter for Mn^{III} than for Fe^{III}, as expected from the general trends (and of course the $Mn^{IV}–O_2H^-$ bond, ~1.83 Å, is much shorter than in the corresponding $Fe^{III}–O_2H$ complexes, 2.21–2.35 Å). On the other hand, the $Mn^{III}–O_2H_2$ bonds (2.40–2.52 Å) are ~0.2 Å longer than the $Fe^{III}–O_2H_2$ (2.25–2.31 Å), owing to the Jahn–Teller effect of Mn^{III}.

Moreover, the $Mn^{III}–O_2^-$ bond (1.88–1.92 Å) is 0.2–0.3 Å shorter than the corresponding $Fe^{III}–O_2^-$ bond (2.10–2.21 Å). The $Fe(Im)_3(Ac)(H_2O)(O_2)$ complex binds O_2^- in a side-on mode, whereas in all the other complexes it binds in a bent end-on mode to the other complexes (cf. Figures 1c and e). Yet, the $Fe–O_{sub}$ bond length does not change at all. Therefore, the difference in the $M^{III}–O_2^-$ bond length is probably caused by the change in spin state from HS in Fe (with all 3*d* orbitals singly occupied) to IS in Mn (with two empty 3*d* orbitals). It is also notable that the spin density on O_2^- is lower (and antiferromagnetically coupled to that on the metal) in the Mn (–1.14 to –1.35 a.u.) than in the Fe complexes (1.35–1.51 a.u.).

On the other hand, the $Mn^{II}–O_2^-$ bond (2.19 Å) is 0.3 Å *longer* than the corresponding $Fe^{II}–O_2^-$ bond (1.86–1.91 Å), except for the dissociative state (with the differing IS $Mn^{III}–O_2^{2-}$ state; 1.85 Å). In all complexes, O_2 binds in an end-on mode. Both metals are in the HS state (except the dissociative Mn complex) with all five 3*d* orbitals occupied. However, the spin densities on O_2^- in the Fe complexes (0.93–0.96 a.u.) are lower than those in the Mn complexes (1.03–1.04 a.u.).

3.3 Energetics of the reactions

In this section, we will study reaction energies in various conceivable reaction steps of the two SOD half-reactions. In particular, we will compare the energies of the two metals and of the dissociative, associative, and second-sphere mechanisms. The energies of all considered reactions are collected in Tables 5–7. For all reactions, we have listed four energies, viz. the pure energy in vacuum without any thermodynamic corrections (ΔE, $\varepsilon = 1$) and the free energy (including zero-point energy and thermal corrections to ΔG at 298 K and 1 atm pressure), either in vacuum ($\varepsilon = 1$) or in a continuum solvent with a dielectric constant (ε) of 4 (a protein-like environment) or 80 (like water). If not otherwise stated, we will only discuss ΔG for $\varepsilon = 4$ and this entry is highlighted in the tables. However, all small molecules (H_2O, OH^-, Im, ImH, or the O_2^--derived ligands) are always assumed to come from bulk water and are therefore studied only at $\varepsilon = 80$ (with or without zero-point and thermal effects).

3.3.1 Resting states

To obtain an estimate of the accuracy of the calculated energies, we will start by looking at two reactions for which experimental data are available. First, we will consider the binding energy of a water ligand to the dissociative complexes, i.e. the reaction

$$M(Im)_3(Ac) + H_2O \rightarrow M(Im)_3(Ac)(H_2O) \qquad (7)$$

All crystal structures of the resting states of Fe and MnSODs have a five-coordinate active site.[22,23,24] Therefore, this reaction should be exergonic. From the two first rows in Table 5, it can be seen that the free energy for this reaction is close to zero: For the Mn^{3+} complexes, it is exergonic by 15 kJ/mole, whereas for the other complexes

complexes, the reaction is actually slightly endergonic, by 11–17 kJ/mole, in variance to the experimental observation of five-coordinate sites also in the reduced proteins.[22, 23]

There are several reasons for this discrepancy. First, the inherent accuracy of the absolute quantum chemical energies is ~25 kJ/mole,[59,60,61,62,63] so the sign of these small energies is not significant. Second, solvation effects have a strong influence on these energies, destabilising the binding as the dielectric constant of the continuum solvent is increased (the reaction is more favourable in vacuum). Since the dielectric constant of a protein is not well defined and may vary from 2 to over 80,[67,68,83] it is hard to decide which value should be used for the SODs. Third, thermal effects are also important for these binding energies and disfavour the binding. The reason for this is that the number of free molecules is reduced from two to one, leading to a strong decrease in the translational entropy. It is well-known that the Sackur–Tetrode equation overestimates this effect in proteins and water solution, but the exact correction factor is not known (we have used a value of 32 kJ/mole, but this may be too small).[58] Finally, the binding of the fifth ligand is stabilised by hydrogen bonds to Gln-69/146 in the proteins, an effect that is not included in the present calculations.

Thus, we can conclude that the absolute values of the binding energies are quite uncertain. However, the *relative* values between the two metals and between various mechanisms (dissociative, associative, or second-sphere) are affected by these uncertainties in the same way (by a constant factor), and therefore can be expected to be much more accurate. The same applies to most energies in this paper. Thus, we can conclude that the binding of the solvent molecule to the active site of Fe and MnSODs is more favourable for Mn than for Fe by 5 kJ/mole in the reduced state and 26 kJ/mole in the oxidised state (note that these two differences vary by at most 4

kJ/mole between the various columns in Tables 5).

Next, we look at the protonation of the solvent molecule in the resting state. Such a reaction is hard to study, because the proton has to be taken from somewhere. In this paper, we have assumed that the proton is taken from neutral imidazole in aqueous solution (which has a pK_a of 7.0;[82] thereby we will experience some cancellation of errors). Thus, we will study the reaction

$$M(Im)_3(Ac)(H_2O) + Im \rightarrow M(Im)_3(Ac)(OH^-) + ImH^+ \quad (8)$$

These types of reactions are collected in Table 6, and from the two first rows, it can be seen that this reaction is exergonic for the oxidised sites (reaction 2) and endergonic for the reduced sites (reaction 1). This suggests that at neutral pH, the oxidised sites should be deprotonated, whereas the reduced sites should be protonated. This is in perfect agreement with the experimental consensus,[3,25] with recent quantum refinement of the crystal structures of MnSOD,[77] and also with earlier calculations.[26,46,47] Therefore, we can conclude that the calculated energies are reasonable and this gives us some confidence to believe the results for reactions, for which experimental data is missing.

3.3.2 Reduction potentials and electron transfer

Next, we turn to the reduction potential of the resting states. In water solution, the Mn^{III}/Mn^{II} potential (+1.51 V) is much more positive than that of Fe^{III}/Fe^{II} (+0.77 V).[3] It has been suggested that the differences in these two reduction potentials may explain why metal-substituted SODs in general are not active.[3] However, the results in Table 7 (reaction 14) show that with the ligands in the active sites of Fe and MnSOD, the difference between Fe and Mn is minimal. In the dissociated state, Mn still has a slightly higher potential than Fe, but only by 0.2 V, but in the associative

and second-sphere models, the difference has essentially disappeared. The same is observed if we allow the electron transfer to be coupled to a (de)protonation of the metal-bound solvent molecule, as is expected in the resting state of the enzymes (i.e. $M^{II}(H_2O) \rightarrow M^{III}(OH) + H^+ + e^-$, reaction 15): we predict the same reduction potential, 0.6 V, for both metals ions. It is notable that this potential is essentially independent of solvent effects (Tables S1-S3) and that the coupled potentials are reasonably similar to the experimental reduction potentials of Fe and MnSOD, 0.22–0.29 V,[3] although the surrounding protein has been modelled only as a featureless continuum. This clearly illustrates that the potentials strongly depend on the first-sphere ligands and that the ligands in the SODs cause Mn and Fe to behave more similar than in bulk solution.

It should be noted that these trends are not an artefact of the calculations: If we calculate the reduction potentials of $M(H_2O)^{2+/3+}$ with the same methods, the difference between Mn and Fe is 0.77 V, i.e. very close to the experimental estimate, 0.74 V.[3]

Both half-reactions of the SODs involve internal electron transfer between the metal and the O_2^- substrate molecule. However, as was discussed in section 3.1, this transfer is spontaneous in all calculations involving both the metal and the substrate: We only obtain a single electronic state (redox state), whereas the other redox state is an excited state that is normally very hard to find and optimise, except when the two redox states have a different number of unpaired spins (as often is the case for Mn) or a different geometry (e.g. first- and second-sphere binding of the substrate). Therefore, no reduction potentials can be given for most of the complexes involving a O_2-derived ligand. The same most likely applies also to the proteins: At the short metal–substrate distances for first- and second-sphere complexes, internal electron

transfer between the metal and the substrate is expected to be instantaneous and not rate limiting.

3.3.3 First half-reaction

We will now turn to the actual reaction mechanism of the SODs, starting with the first half-reaction in Eqn. (4). The relevant reaction energies are collected in Table 7. For each reaction, five entries are given for each metal, viz. energies for the dissociative complexes, the associative complexes with H_2O (or AcH–OH), the associative complexes with OH, the second-sphere complexes with H_2O (or AcH–OH), and the second-sphere complexes with OH. All energies in Table 7 are ΔG in a protein-like continuum solvent with $\varepsilon = 4$. In supplementary material, the corresponding results in vacuum and in water are given, as well as the vacuum results without any thermodynamic corrections (Tables S1–S3). In this section and the next, we will concentrate on the associative and second-sphere mechanisms, in which the metal-bound solvent molecule can be involved in the necessary proton transfers. The dissociative mechanism will be considered in Section 3.3.4.

The first half-reaction starts with the binding of O_2^- to the oxidised resting state. This reaction (#3 in Table 7) is exergonic (by 19–243 kJ/mole) for both metals and all binding modes. This is related to the positive net charge of the metal site (+1 with OH^- and +2 with H_2O), which is also reflected in the lower binding energy to the complexes with OH^- (the expected protonation state), –19 to –52 kJ/mole. The associative O_2^- complex is 21–25 kJ/mole more stable than the second-sphere complex for both metals.

The first half-reaction of the SODs is simply the transfer of an electron in O_2^- to M^{III}. As we saw in section 3.1, this transfer occurs spontaneously when the ligand

starts to dissociate and forms second-sphere complexes. Therefore, we can in principle imagine the direct dissociation of $^3O_2$ from the reduced complex again. This is the reverse of reaction 1 in Table 7. It can be seen that the dissociation of $^3O_2$ is endergonic for the expected hydroxide complexes (by 4–24 kJ/mole), except the second-sphere complex with Fe.

However, the consensus is that the active site should take up a proton during this half-reaction, by protonating the solvent molecule in the reduced site. This protonation can take place after the dissociation of the oxygen molecule and we have already seen that such a protonation is favourable at neutral pH (reaction 2 in Table 6). Yet, it is also possible that protonation takes place when O_2^- is still bound (the reverse of reactions 5–6 in Table 6). It can be seen that it is favourable (as usual compared to the protonation of Im) for both metals in both the associative and second-sphere complexes (by 7–64 kJ/mole). Thus, it is likely that the proton is taken up before the dissociation of $^3O_2$, especially as such a protonation will make the dissociation exergonic for all complexes (by 4–40 kJ/mole; the reverse of reaction 1 in Table 7). Thus, our results confirm the suggestion[84] that protonation of the hydroxide ligand will enhance the product formation.

Finally, it is also conceivable that the proton is provided already at the binding, i.e. that O_2^- is protonated to HO_2 before the binding to the metal. From Table 7 (reaction 5), it can be seen that this binding is endergonic for the associative hydroxide complexes (by 20-71 kJ/mole), but slightly exergonic for the second-sphere Mn complex (by 6 kJ/mole). Such a binding should be followed by an internal proton transfer from HO_2 to OH^-, which is exergonic by 96–136 kJ/mole (reaction 11 in Table 7). For the second-sphere Fe complex, these two reactions occur spontaneously, and no separate $Fe(Im)_3(Ac)(OH)+HO_2$ could be found. Moreover,

considering that the pK_a of HO_2 is 4.9,[82] such a reaction mechanism is less likely than the direct binding of O_2^- (protonation of O_2^- would cost ~13 kJ/mole in energy terms,[85] which would make the binding of HO_2 unfavourable for all hydroxide complexes. On the other hand, the results show that the $[M(H_2O)(O_2)]^{2+}$ tautomer is 46–101 kJ/mole more stable than the $[M(OH)(HO_2)]^{2+}$ tautomer.

Thus, we can conclude that the first half-reaction of Fe and MnSODs is quite facile and down-hill for both metals. The results indicate that the associative mechanism is more favourable than the second-sphere mechanism and that the OH^- ligand is protonated before O_2 is released.

3.3.4 Second half-reaction

We will now turn to the second half-reaction of the SODs, Eqn. (5) above. Again, it starts with the binding of O_2^-, but this time to the reduced complex. From Table 7 (reaction 2) it can be seen that this binding is slightly exergonic (by 2–11 kJ/mole) for the expected H_2O complexes, except for the associative Fe complex (endergonic by 2 kJ/mole).

Next, O_2^- should accept two protons before it dissociates as H_2O_2. One of the protons should come from the water ligand, the other from the surroundings, but the order of these two transfers is not known, so we will study both possibilities, starting with the uptake of a proton from the surroundings first. From Table 7, it can be seen that this reaction (# 8) is exergonic for the associative water complexes (by 15–42 kJ/mole), but endergonic for the second-sphere Mn complex (by 14 kJ/mole). The second-sphere Fe complex with HO_2 is not stable, but automatically reorganises to the $Fe^{III}(Im)_3(Ac)(OH)]^+ + H_2O_2$ product complex in a slightly endergonic reaction (by 2 kJ/mole; naturally, similar results are obtained for the direct binding of HO_2, taking

into account the unfavourable protonation of O_2^- in water solution). This reaction would then be followed by an internal proton transfer from H_2O to HO_2. Interestingly, this reaction (# 12) is predicted to be favourable only for the second-sphere Mn complex (by 7 kJ/mole; but this is not the stable state in our calculations). In the first coordination sphere, the reaction is endergonic by 38–40 kJ/mole.

Alternatively, the internal proton transfer (from H_2O to O_2^-) occurs first. From reaction 13 in Table 7, it can be seen that it is unfavourable for all water complexes by 7–80 kJ/mole. This would then be followed by an uptake of a proton from the surroundings (reaction 10), which is exergonic for all complexes (by 0-59 kJ/mole) Thus, both alternatives give at least one endergonic reaction, but the energies are small. For Fe, the most favourable path is to bind O_2^- in the second sphere (exergonic by 2 kJ/mole and 4 kJ/mole more favourable than first-sphere binding), followed by the uptake of an external proton, which leads directly to the product complex in an endergonic reaction by only 2 kJ/mole. For Mn, the most favourable path is to bind O_2^- in the first sphere (exergonic by 11 kJ/mole and 7 kJ/mole more favourable than first-sphere binding), followed by an internal proton transfer, during which HO_2 moves to the second sphere (endergonic by 14 kJ/mole, 7 of which comes from the change in the coordination mode; second-sphere coordination is now favourable by 66 kJ/mole), and then an uptake of an external proton, which is thermoneutral.

Finally, H_2O_2 should dissociate from the $[M^{III}(Im)_3(Ac)(OH)(H_2O_2)]^+$ complex (for which the associative and second-sphere forms are almost equally stable, indicating that the dissociation of the product starts spontaneously). According to Table 7, this reaction (the reverse of reaction 7) is slightly exergonic (by 7–17 kJ/mole) for the relevant OH^- complexes.

In conclusion, our results indicate that the second half-reaction is more

favourable for (at least partly) second-sphere mechanism. The most favourable order of the two proton transfers differs for the two metals. It includes one endergonic reaction, but only by 2–14 kJ/mole. Such reaction energies are within the error limits of the method and they are also compatible with the experimental turn-over rate, ~$4 \cdot 10^4$ s^{-1} (corresponding to an activation energy of ~50 kJ/mole).[3,4]

3.3.5 Dissociative mechanisms

We now turn to the dissociative mechanism, which involves dissociation of the metal-bound solvent molecule. The binding energies of H_2O to all types of complexes are listed in Table 5. It can be seen that this reaction is close to thermoneutral for all complexes (less than 20 kJ/mole). Considering the uncertainty in these energies, discussed for the resting states above, this means that we cannot with certainty say that any water complex prefers the dissociative state. In the same table, we also study the corresponding binding energies of OH^- for the various complexes (to make the energies consistent and to take into account the low concentration of OH^- in water at pH 7, this reaction was modelled as the binding of H_2O, followed by its deprotonation by ImH). It can be seen that the binding of OH^- is favourable for all the oxidised complexes (formally M^{III}), except perhaps $[M(Im)_3(Ac)(O_2)]^+$ (endergonic by 15-16 kJ/mole).

With this in mind, we can now look at the details of the dissociative mechanism, starting with the first half-reaction. The resting M^{III} state is most likely $M^{III}(OH)$. It is unlikely that this complex will loose the OH^- ligand or that it will be protonated. Therefore, the binding of O_2^- should proceed along the associative or second-sphere pathway (which we have seen is strongly favourable). From Table 5 (reaction 12) it may seem that the resulting $M(Im)_3(Ac)(OH)(O_2)$ complex may

dissociate OH^- (exergonic by 15–16 kJ/mole). However, this is mostly because the uptake of a proton is favourable (Table 6, the reverse of reactions 5 and 6; by 7–64 kJ/mole). Once the complex is protonated, the dissociation of H_2O is nearly thermoneutral (–8 to +11 kJ/mole; Table 5, reaction 5). On the other hand, the dissociation of $^3O_2$ is exergonic, as we have seen. Therefore, we conclude that the dissociative mechanism is unlikely for the first half-reaction of the Fe and MnSODs.

Next, we turn to the second half-reaction, in which $M^{II}(H_2O)$ binds O_2^-. We have already seen that our calculations predict that the dissociation of water actually is slightly exergonic (by 12–17 kJ/mole). Even if this is not in agreement with the crystal structures, it shows that water binds rather weakly to this complex. After the binding of O_2^-, the dissociation energy of H_2O is similar (7 to –20 kJ/mole; reaction 4 in Table 5), making it hard to decide whether the dissociative mechanism is a competitive alternative or not.

However, if we assume that the dissociative $M(Im)_3(Ac)(O_2)$ complex actually forms, it should then take up a proton to form $[M(Im)_3(Ac)(HO_2)]^+$, a reaction that is exergonic by 28–32 kJ/mole (reaction 8 in Table 7). This complex must then take up another proton, because the dissociation of HO_2^- is strongly unfavourable (by 264–268 kJ/mole; the reverse of reaction 6 in Table 7). This uptake is reaction 10 in Table 7, but it is also strongly endergonic (by 207–223 kJ/mole). Therefore, the reaction cannot continue along the dissociative pathway. Instead, the $[M(HO_2)]^{2+}$ complex needs to take up H_2O, which is nearly thermoneutral according to reaction 6 in Table 6 (by –7 to + 6 kJ/mole). It can then follow the associative or second-sphere pathways as discussed above.

Thus, we can conclude that at least parts of both half-reactions of Fe and MnSOD must proceed along the associative or second-sphere pathways. We cannot

(considering the estimated accuracy of the method) discard the possibility that dissociative complexes arise in some of the steps of the reaction, but this would only make the reactions more complicated (the solvent molecule dissociates and binds again), without any gain in the reaction energies. Moreover, dissociative mechanisms cannot exploit the attractive possibility of using the metal-bound solvent molecule as a storage for one of the protons involved in the mechanism.

3.4 Spin considerations

The O_2^- substrate molecule has an unpaired electron, whereas the products have no (H_2O_2) or two (O_2) unpaired electrons. It is therefore of interest to study how the spins are conserved throughout the reactions, especially as the spin preferences of the two metals differ and the reactions are very fast.

Iron always prefers the HS state. Therefore, all reactions will preserve the spin if the incoming O_2^- substrate radical has the same direction of its unpaired spin as the metal. If this is not the case, a single spin flip is needed for both half-reactions. It remains to be demonstrated if the spin–orbit coupling of Fe is large enough to allow for a reaction rate close to the diffusion limit. Such spin flips have been studied for some related Fe–O_2 systems[86,87] and for these, the rate for the spin conversion depends on the slope of the potential surfaces for the two relevant spin states at the crossing point. A small spin splitting energy, as observed for the oxidised resting state in our models (Table 1), is favourable for the spin conversion.

For Mn, the situation is more complicated because the preferred spin states vary more. For the first half-reaction, the metal and the substrate together have either three or five unpaired spins. On the other hand, Mn^{II} and $^3O_2$ have together seven or three unpaired spins. Therefore, O_2^- should have the opposite spin of the metal in order to

avoid spin conversion. From Table 2 it can also be seen that the $[Mn(O_2)]^{2+}$ intermediate is also most stable with three unpaired spins in the preferred associative complexes. However, in the second-sphere complexes, the HS state with seven unpaired electrons is lower in energy.

For the second half-reaction, the situation is similar: The two reactants have four or six unpaired spins, whereas the products have four unpaired spins. Therefore, O_2^- should again have the opposite spin of the metal to avoid spin crossing. The intermediate $[Mn(H_2O_2)]^{2+}$ complex is most stable with four unpaired spins, whereas the preferred spin state of the other two intermediates $[Mn(O_2)]^+$ and $[Mn(HO_2)]^{2+}$ depends on the coordination mode, although the state with four unpaired spins is either most favourable or close in energy to the lowest spin state. This degeneracy also provides an appropriate means for the spin conversion, needed if the spin of O_2^- is parallel to that of the metal complex. Thus, our results indicate that the most likely mechanism coincides with close-lying spin states. Therefore, we suggest that these reactions have been designed to facilitate spin crossover, when necessary, by employing the same design principle as suggested for haem proteins.[86]

3.5 Conclusions

In this paper, we have studied the two half-reactions of Fe and MnSODs using small quantum chemical models of the active site. In particular, we have compared the properties of the two metal ions and contrasted three possible reaction mechanisms, dissociative, associative, and second sphere. This has given several interesting conclusions.

We have seen that for the first half-reaction (Eqn. 4), an associative mechanism is steadily down-hill. In particular, we have seen that when O_2^- binds to M^{III}, it

automatically donates some charge to the metal, so that it becomes a mixture of $^2O_2^-$ and $^3O_2$. Moreover, it binds only weakly to the metal, and when the solvent ligand becomes protonated, the dissociation of $^3O_2$ is exergonic.

For the second half-reaction (Eqn. 5), the results are less clear. It seems that both metals prefer second-sphere complexes at least for some of the intermediates. Moreover, the preferred order of the internal and external proton transfer seems to differ between the two metals. The reactions also involve one endergonic step for both metals, but only by 2–14 kJ/mole. Such steps are fully consistent with the observed kinetic rates (k_{cat} = 2.6–4·10^4 s^{-1} [3,4]), which correspond to activation barriers of 47–48 kJ/mole. However, many of the energies involved are small so the conclusions are somewhat uncertain. In particular, we cannot fully discard a dissociative mechanism on the basis of energies, even if it is more complicated. The suggested mechanisms for the two half-reactions of FeSOD are shown in Figure 2. Note that the energy of the total reaction, Eqn. (1), is exothermic by 105 kJ/mole, if the protons are assumed to come from Im, independent on the enzyme, and that almost all of this energy is gained in the first half-reaction.

As mentioned in the introduction, experimental evidence on the coordination mode of the O_2-derived ligand is based only on the binding of non-native ligands (like NO, N_3^- and F^-) to the protein. This has provided somewhat contradictory evidence for both associative, dissociative, and second-sphere mechanisms.[3,32,33,34,35,36,37,38,39,40] The present investigation complements these results by providing calculations on the intermediates expected in the reaction mechanism. Our results suggest an associative mechanism for the first half-reaction, in accordance with the experimental observation of six-coordinate N_3^- and F^- complexes to the oxidised protein.[3,23,40] On the other hand, we suggest a (partly) second-sphere mechanism for the second half-reaction, in

agreement with the observation that N_3^- and F^- do not bind directly $Fe^{II}SOD$[37], However, six-coordinate complexes have been observed for NO with $Fe^{II}SOD$[33] and N_3^- and F^- with $Mn^{II}SOD$,[34] which has been taken as an evidence for a associative mechanism for the second half-reaction.[3] This indicates that the associative and second-sphere complexes have similar energies, in agreement with our observations. In particular, we find a stronger preference of second-sphere binding for Fe than for Mn for the $[M(Im)_3(AcH)(OH)(HO_2)]^{2+}$ state, in agreement the experimental results for N_3^- and F^-.[34,37] It is notable that a second-sphere binding of the substrate to the reduced state is compatible with the observation that the metal-bound water in this complex has one proton that is not employed in any hydrogen bond in the crystal structure (in variance to the hydroxide ion in the oxidised complex).[77] This may be an ingenious mechanism to stabilise the second-sphere binding, which intrinsically has lower reaction energies, according to our results.

Our calculations indicate that Fe and Mn have quite similar properties and energetics. There are some small differences in the preferred oxidation states between the two metals. In particular, the +IV state is more accessible for Mn than for Fe. Moreover, all Fe complexes are most stable in the high-spin states, whereas some of the Mn complexes are more stable in the IS states. We have seen that this leads to a favourable spin chemistry of the reactions.

There are also some differences in the optimum geometries of the two metals. In particular, the Fe^{II} complexes have somewhat shorter bond lengths than the corresponding Mn^{II} complexes, whereas the opposite is true for the M^{III} complexes. Moreover, Mn^{III} has a much stronger tendency to form the AcH–OH tautomer of the water complexes than Fe. Finally, the $[Fe(Im)_3(Ac)(H_2O)(O_2)]^+$ binds O_2 in the side-on mode, whereas O_2^- prefers to bind end-on in corresponding Mn complex.

There are a few conspicuous differences between the energies of Fe and Mn. First, Mn seems to bind H_2O stronger than Fe by 5–27 kJ/mole (except for the $[M(Im)_3(Ac)(H_2O)(O_2)]^+$ complex mentioned above; Table 5). Second, the deprotonation energies of H_2O are more positive for Mn than for Fe by 2–54 kJ/mole, with the same exception (Table 6). Third, both O_2^- and $^3O_2$ binds stronger to Mn than Fe by 8–29 kJ/mole (again with the same exception, reactions 1 and 3 in Table 7). Finally, reaction 9 in Table 7 is more endergonic for Mn than for Fe by 11–58 kJ/mole. However, for all the other reactions, no clear trends are found between the two metals.; instead, the energies are similar with differing trends in the various coordination modes.

The most interesting energetic result is that although the reduction potentials of the two metals differ by 0.7 V in water solution, the difference for SOD active-site models is minimal. This explains why the two proteins may be so similar. However, it does not explain why the reduction potential of metal-substituted Fe/MnSODs changes by 0.5–0.7 V,[3] but it has been suggested that these shifts are caused by interactions with second-sphere protein residues.[43] We currently investigate this, as well as the full reaction mechanism, with combined quantum and molecular mechanics (QM/MM) methods, involving the whole protein.

Acknowledgements

This investigation has been supported by the Swedish research council, by computer resources of Lunarc at Lund University, and by the project LC512 of MSMT CR (LR).

Table 1. Spin-splitting energies ($\Delta E_{spin,}$ kJ/mole) and spin densities on iron and O_2, HO_2, or H_2O_2 (ρ, a.u.) of the studied iron models. "To Im" indicates that the substrate molecule forms a hydrogen bond to the Im ligands, rather than to the solvent molecule.

Model	M_s	ΔE_{spin}	ρ (Fe)	ρ (substrate)
Fe^{II}				
$[Fe^{II}(Im)_3(Ac)]^+$	0	118	-0.07	
Ac bidentate	1	68	2.04	
	2	0	3.88	
$[Fe^{II}(Im)_3(Ac)(H_2O)]^+$	0	106	0.02	
	1	71	2.03	
	2	0	3.88	
$Fe^{II}(Im)_3(Ac)(OH)$	0	104	0.01	
	1	62	2.06	
	2	0	3.80	
Fe^{III}				
$[Fe^{III}(Im)_3(Ac)]^{2+}$	1/2	80	1.02	
Ac bidentate	3/2	29	2.93	
	5/2	0	4.34	
$[Fe^{III}(Im)_3(AcH)(OH)]^{2+}$	1/2	89	1.10	
	3/2	18	2.97	
	5/2	0	4.34	
$[Fe^{III}(Im)_3(Ac)(OH)]^+$	1/2	86	0.89	
	3/2	21	2.71	
	5/2	0	4.09	
$Fe^{III}–H_2O_2$				
$[Fe^{III}(Im)_3(Ac)(H_2O_2)]^{2+}$	1/2	31	1.06	-0.01
Ac bidentate	3/2	27	2.90	0.03
	5/2	0	4.33	0.05
$[Fe^{III}(Im)_3(AcH)(OH)(H_2O_2)]^{2+}$	1/2	29	1.04	-0.01
	3/2	9	3.04	0.03
	5/2	0	4.39	0.06
$[Fe^{III}(Im)_3(Ac)(OH)(H_2O_2)]^+$	1/2	79	0.92	-0.01
	3/2	35	2.92	0.00
	5/2	0	4.28	0.02
$[Fe^{III}(Im)_3(AcH)(OH)]^{2+}+H_2O_2$	1/2	83	1.04	0.00
	3/2	20	2.97	0.00
	5/2	0	4.35	0.00
$[Fe^{III}(Im)_3(Ac)(OH)]^+ + H_2O_2$	1/2	98	1.07	0.01
	3/2	32	2.92	0.00
	5/2	0	4.26	0.01
$Fe^{III}–O_2^- = Fe^{II}–O_2$				
$[Fe(Im)_3(Ac)(O_2)]^+$	0	92	1.07	-0.97
Ac bidentate	1	42	3.13	-1.19
	2	45	3.79	-0.19
	3	0	4.10	1.53
$[Fe(Im)_3(Ac)(H_2O)(O_2)]^+$	0	27	1.05	-0.95
O_2 side on	1	50	1.07	1.00

Model	M_s	ΔE_{spin}	ρ (Fe)	ρ (substrate)
	2	36	4.09	-0.43
	3	0	4.20	1.51
$Fe(Im)_3(Ac)(OH)(O_2)$	0	22	1.01	-0.99
	1	35	1.03	0.93
	2	35	3.03	0.80
	3	0	4.18	1.35
$[Fe(Im)_3(Ac)(H_2O)+O_2]^+$	0	60	2.03	-1.99
	1	99	0.01	1.97
	2	74	2.08	1.93
	3	0	3.93	1.92
$[Fe(Im)_3(Ac)(OH)+O_2]^0$	0	121	0.52	-0.63
Ac bidentate	1	18	3.58	-1.76
	2	64	3.48	0.35
	3	0	3.89	1.68
$Fe^{III}–HO_2$				
$[Fe(Im)_3(Ac)(HO_2)]^{2+}$	0	45	-0.81	0.73
Ac bidentate	1	27	1.61	0.53
	2	63	3.25	0.46
	3	0	4.29	0.95
$[Fe(Im)_3(AcH)(OH)(HO_2)]^{2+}$	0	43	0.70	-0.71
	1	23	1.63	0.42
	2	50	3.44	0.33
	3	0	4.36	1.02
$[Fe(Im)_3(Ac)(OH)(HO_2)]^+$	0	62	0.90	-0.94
	1	29	1.74	0.15
	2	29	3.44	0.08
	3	0	4.23	1.01
$[Fe(Im)_3(Ac)(H_2O)+HO_2]^{2+}$	0	86	1.13	-1.00
	1	87	1.00	1.00
	2	92	2.93	1.00
	3	0	4.35	1.01
$[Fe(Im)_3(Ac)(OH)+HO_2]^+$	0	35	1.04	-1.00
Ac bidentate	1	88	1.06	1.01
	2	50	2.85	1.01
	3	0	4.25	1.03
$Fe^{II}–O_2^-$				
$Fe(Im)_3(Ac)(O_2)$	1/2	98	0.26	0.72
Ac bidentate	3/2	72	2.34	0.69
	5/2	0	3.83	0.94
$Fe(Im)_3(Ac)(H_2O)(O_2)$	1/2	38	0.28	0.76
	3/2	41	2.75	0.20
	5/2	0	3.92	0.93
$[Fe(Im)_3(Ac)(OH)(O_2)]^-$	1/2	71	0.69	0.34
	3/2	40	3.24	-0.40
	5/2	0	3.76	0.96
$[Fe(Im)_3(Ac)(H_2O)+O_2]^0$	1/2	45	2.07	-1.00
	3/2	73	2.05	1.00
	5/2	0	3.87	1.00

Model	M_s	ΔE_{spin}	ρ (Fe)	ρ (substrate)
$[Fe(Im)_3(Ac)(OH)+O_2]^-$	1/2	82	2.06	-0.98
to Im	3/2	77	2.05	1.00
	5/2	0	3.77	0.99
$Fe^{II}–HO_2 = Fe^{III}–HO_2^-$				
$[Fe(Im)_3(Ac)(HO_2)]^+$	1/2	24	0.92	0.15
Ac bidentate	3/2	27	2.82	0.10
	5/2	0	4.14	0.38
$[Fe(Im)_3(AcH)(OH)(HO_2)]^+$	1/2	7	0.94	0.13
	3/2	22	2.85	0.00
	5/2	0	4.21	0.39
$Fe(Im)_3(Ac)(OH)(HO_2)$	1/2	32	0.97	0.06
	3/2	35	2.80	0.03
	5/2	0	4.15	0.36
$[Fe(Im)_3(Ac)(H_2O)+(HO_2)]^+$	1/2	61	2.05	-1.00
to Im	3/2	0	3.89	-0.99
	5/2	0	3.91	0.95
$Fe(Im)_3(Ac)(OH)+(HO_2)$	1/2	82	1.05	-0.06
	3/2	45	3.24	-0.30
	5/2	0	3.81	1.00

Table 2. Spin-splitting energies ($\Delta E_{spin,}$ kJ/mole) and spin densities on iron and O_2, HO_2, or H_2O_2 (ρ, a.u.) of the studied manganese models.

Model	M_s	ΔE_{spin}	ρ (Mn)	ρ(substrate)
Mn^{II}				
$[Mn^{II}(Im)_3(Ac)]^+$	1/2	198	1.02	
Ac bidentate	3/2	131	3.18	
	5/2	0	4.97	
$[Mn^{II}(Im)_3(Ac)(H_2O)]^+$	1/2	203	1.08	
	3/2	127	3.25	
	5/2	0	4.98	
$Mn^{II}(Im)_3(Ac)(OH)$	1/2	208	1.15	
	3/2	122	3.17	
	5/2	0	4.91	
Mn^{III}				
$[Mn^{III}(Im)_3(Ac)]^{2+}$	0	135	-0.02	
Ac bidentate	1	101	2.13	
	2	0	4.11	
$[Mn^{III}(Im)_3(AcH)(OH)]^{2+}$	0	160	0.00	
	1	119	2.12	
	2	0	4.11	
$[Mn^{III}(Im)_3(Ac)(OH)]^+$	0	160	0.10	
	1	122	2.08	
	2	0	4.01	
$Mn^{III}–H_2O_2$				
$[Mn^{III}(Im)_3(Ac)(H_2O_2)]^{2+}$	0	114	-0.01	0.00
Ac bidentate	1	62	2.15	-0.02
	2	0	4.17	0.02
$[Mn^{III}(Im)_3(AcH)(OH)(H_2O_2)]^{2+}$	0	130	-0.04	0.00
	1	77	2.14	-0.01
	2	0	4.20	0.03
$[Mn^{III}(Im)_3(Ac)(OH)(H_2O_2)]^+$	0	144	0.03	0.00
	1[a]	118	2.06	0.00
	2	0	4.06	0.01
$[Mn^{III}(Im)_3(AcH)(OH)]^{2+}+H_2O_2$	0	160	-0.01	0.00
	1	124	2.14	0.00
	2	0	4.14	0.00
$[Mn^{III}(Im)_3(Ac)(OH)]^+ + H_2O_2$	0	158	0.06	0.01
	1	115	2.10	0.01
	2	0	4.00	0.00
$Mn^{III}–O_2^- = Mn^{II}–O_2$				
$[Mn(Im)_3(Ac)(O_2)]^+$	1/2	54	2.06	-0.97
Ac bidentate	3/2	0	4.26	-1.21
	5/2	21	4.09	0.94
$[Mn(Im)_3(Ac)(H_2O)(O_2)]^+$	1/2	66	2.14	-0.99
	3/2	0	4.36	-1.35
	5/2	25	4.35	0.63
$Mn(Im)_3(Ac)(OH)(O_2)$	1/2	67	2.04	-0.98
	3/2	0	4.13	-1.14

Model	M_s	ΔE_{spin}	ρ (Mn)	ρ(substrate)
	5/2	15	4.10	0.87
$[Mn(Im)_3(Ac)(H_2O)+O_2]^+$	1/2	131	3.23	-1.99
	3/2	33	4.90	-1.90
	5/2	83	4.01	0.99
	7/2	0	4.98	1.99
$[Mn(Im)_3(Ac)(OH)+O_2]^0$	1/2	141	1.90	-0.98
Ac bidentate	3/2	26	4.58	-1.64
	5/2	67	3.93	1.03
	7/2	0	4.81	1.96
$Mn^{III}–HO_2$				
$[Mn(Im)_3(Ac)(HO_2)]^{2+}$	1/2	68	1.75	-0.60
Ac bidentate	3/2	-22	2.96	0.22
	5/2	0	4.08	1.01
$[Mn(Im)_3(AcH)(OH)(HO_2)]^{2+}$	1/2	62	1.89	-0.78
	3/2	-10	3.08	0.07
	5/2	0	4.13	1.01
$[Mn(Im)_3(Ac)(OH)(HO_2)]^+$	1/2	76	1.27	-0.21
	3/2	-25	3.80	-0.74
	5/2	0	4.04	0.99
$[Mn(Im)_3(AcH)(OH)+HO_2]^{2+}$	1/2	117	2.16	-1.00
	3/2	27	4.15	-1.00
	5/2	0	4.09	1.00
$[Mn(Im)_3(Ac)(OH)+HO_2]^+$	1/2	48	2.08	-1.00
	3/2	0	3.99	-1.00
	5/2	0	4.02	1.00
$Mn^{II}–O_2^-$				
$Mn(Im)_3(Ac)(O_2)$	0	179	0.22	-0.22
Ac bidentate	1	133	2.57	-0.43
	2	-31	4.52	-0.56
	3	0	4.87	1.08
$Mn(Im)_3(Ac)(H_2O)(O_2)$	0	153	-0.09	0.06
	1	73	2.02	0.11
	2	33	4.49	-0.51
	3	0	4.92	1.04
$[Mn(Im)_3(Ac)(OH)(O_2)]^-$	0	108	0.15	-0.17
	1	100	2.13	0.01
	2	6	4.27	-0.36
	3	0	4.84	1.03
$[Mn(Im)_3(Ac)(H_2O)+O_2]^0$	0	202	1.11	-1.00
	1	124	3.15	-1.00
	2	0	4.95	-0.99
	3	0	4.94	1.00
$[Mn(Im)_3(Ac)(OH)+O_2]^-$	0	199	-1.05	1.00
to Im	1	124	3.19	-0.98
	2	3	4.89	-0.99
	3	0	4.87	0.99
$Mn^{II}–HO_2 = Mn^{III}–HO_2^-$				
$[Mn(Im)_3(Ac)(HO_2)]^+$	0	49	0.01	0.02

Model	M_s	ΔE_{spin}	ρ (Mn)	ρ(substrate)
Ac bidentate	1	-6	2.08	0.07
	2	-59	4.05	-0.13
	3	0	4.98	1.00
$[Mn(Im)_3(Ac)(H_2O)(HO_2)]^+$	0	82	0.03	-0.02
	1	23	2.60	-0.39
	2	-81	4.07	-0.10
	3	0	4.93	0.99
$Mn(Im)_3(Ac)(OH)(HO_2)$	0[a]	35	0.66	-0.62
	1	-54	2.09	0.02
	2	-108	4.12	-0.14
	3	0	4.86	0.71
$[Mn(Im)_3(Ac)(H_2O)+HO_2]^+$	0	205	1.05	-0.98
	1	134	3.12	-0.98
	2	6	5.00	-1.00
	3	0	4.98	1.00
$Mn(Im)_3(Ac)(OH)+HO_2$	0	200	1.13	-0.99
	1	218	1.10	0.99
	2	-1	4.95	-1.00
	3	0	4.95	1.01

[a] This state has a different protonation state than that of the most stable spin state.

Table 3. Equilibrium bond lengths (in Å) of metal-coordinating ligands in ground-state Fe models. In addition, data for the crystal structures with the best resolution of reduced and oxidised FeSOD have been included (1.8 and 1.6 Å resolution, respectively).[23,24]

Model	M_s	Fe–N_{ax}	Fe–N_2	Fe–N_3	Fe–O_{Ac}	Fe–O_{Sol}	Fe–O_{Sub}
$[Fe^{II}(Im)_3(Ac)]^+$	2	2.11	2.07	2.07	2.04,2.29		
$[Fe^{II}(Im)_3(Ac)(H_2O)]^+$	2	2.16	2.11	2.10	1.98	2.21	
$Fe^{II}(Im)_3(Ac)(OH)$	2	2.35	2.18	2.17	2.06	1.90	
Fe^{II}SOD (1isa)[23]		2.19	2.12	2.03	1.92	2.06	
second subunit		2.18	2.11	2.03	1.92	2.06	
$[Fe^{III}(Im)_3(Ac)]^{2+}$	5/2	2.07	2.03	2.03	2.06,2.09		
$[Fe^{III}(Im)_3(AcH)(OH)]^{2+}$	5/2	2.05	2.11	2.12	2.03	1.92	
$[Fe^{III}(Im)_3(Ac)(OH)]^+$	5/2	2.24	2.11	2.11	1.95	1.85	
Fe^{III}SOD (1coj)[24]		2.17	2.13	2.09	1.95	2.00	
$[Fe^{III}(Im)_3(Ac)(H_2O_2)]^{2+}$	5/2	2.11	2.08	2.09	2.08,2.11		2.31,3.16
$[Fe^{III}(Im)_3(AcH)(OH)(H_2O_2)]^+$	5/2	2.16	2.11	2.13	2.02	1.99	2.28,3.12
$[Fe^{III}(Im)_3(Ac)(OH)(H_2O_2)]^+$	5/2	2.21	2.18	2.17	2.04	1.86	2.25,3.41
$[Fe^{III}(Im)_3(AcH)(OH)]^{2+}+H_2O_2$	5/2	2.10	2.07	2.06	2.12	1.89	4.88
$[Fe^{III}(Im)_3(Ac)(OH)]^+ + H_2O_2$	5/2	2.24	2.11	2.11	1.95	1.85	4.09
$[Fe(Im)_3(Ac)(O_2)]^+$ asym	3	2.16	2.14	2.14	2.11,2.13		2.10,3.14
$[Fe(Im)_3(Ac)(H_2O)(O_2)]^+$	3	2.14	2.17	2.19	2.07	2.15	2.20,2.22
$Fe(Im)_3(Ac)(OH)(O_2)$	3	2.33	2.11	2.20	1.99	1.88	2.21,3.18
$[Fe(Im)_3(Ac)(H_2O)+O_2]^+$	3	2.18	2.11	2.11	1.97	2.09	4.41
$[Fe(Im)_3(Ac)(OH)+O_2]^0$	3	2.34	2.23	2.21	2.19,2.20	1.87	4.30
$[Fe(Im)_3(Ac)(HO_2)]^{2+}$	3	2.13	2.09	2.09	2.07,2.10		2.21,2.94
$Fe(Im)_3(AcH)(OH)(HO_2)]^{2+}$	3	2.09	2.15	2.13	2.08	1.91	2.35,3.03
$[Fe(Im)_3(Ac)(OH)(HO_2)]^+$	3	2.20	2.17	2.15	1.91	1.87	2.69,3.80
$[Fe(Im)_3(Ac)(H_2O)+HO_2]^{2+}$	3	2.07	2.10	2.13	1.91	2.05	4.32
$[Fe(Im)_3(Ac)(OH)+HO_2]^+$	3	2.12	2.17	2.17	2.14,2.14	1.92	4.03
$Fe(Im)_3(Ac)(O_2)$	5/2	2.21	2.18	2.20	2.12,2.33		1.86,3.08
$Fe(Im)_3(AcH)(OH)(O_2)$	5/2	2.20	2.27	2.26	2.10	2.14	1.91,3.09
$[Fe(Im)_3(Ac)(OH)(O_2)]^-$	5/2	2.26	2.29	2.29	2.37	1.96	1.88,3.11
$[Fe(Im)_3(Ac)(H_2O)+O_2]^0$	5/2	2.20	2.12	2.13	2.03	2.09	4.05
$[Fe(Im)_3(Ac)(OH)+O_2]^-$	5/2	2.25	2.11	2.11	2.26	1.89	4.31
$[Fe(Im)_3(Ac)(HO_2)]^+$	5/2	2.14	2.17	2.17	2.04,2.29		1.90,2.91
$[Fe(Im)_3(Ac)(H_2O)(HO_2)]^+$	5/2	2.20	2.18	2.18	2.20	1.97	1.92,2.82
$Fe(Im)_3(Ac)(OH)(HO_2)$	5/2	2.24	2.22	2.22	2.08	1.87	2.12,3.32
$[Fe(Im)_3(Ac)(H_2O)+HO_2]^+$	5/2	2.16	2.10	2.09	1.95	2.19	4.56
$[Fe(Im)_3(Ac)(OH)+HO_2]^0$	5/2	2.28	2.13	2.18	2.05	1.90	4.07

Table 4. Equilibrium bond lengths (in Å) of metal-coordinating ligands in ground-state Mn models. In addition, data for the crystal structures with the best resolution of reduced and oxidised MnSOD have been included (0.9 Å resolution).[22]

Model	M_s	Mn–N_{ax}	Mn–N_2	Mn–N_3	Mn–O_{Ac}	Mn–O_{Sol}	Mn–O_{Sub}
$[Mn^{II}(Im)_3(Ac)]^+$	5/2	2.18	2.14	2.15	2.13,2.14		
$[Mn^{II}(Im)_3(Ac)(H_2O)]^+$	5/2	2.23	2.20	2.17	2.05	2.23	
$Mn^{II}(Im)_3(Ac)(OH)$	5/2	2.34	2.28	2.28	2.08	1.98	
Mn^{II}SOD (1ixb)[22]		2.18	2.15	2.13	2.04	2.26	
second subunit		2.17	2.14	2.13	2.05	2.28	
$[Mn^{III}(Im)_3(Ac)]^{2+}$	2	1.99	2.04	2.04	1.93,2.10		
$[Mn^{III}(Im)_3(AcH)(OH)]^{2+}$	2	2.03	2.06	2.06	2.07	1.85	
$[Mn^{III}(Im)_3(Ac)(OH)]^+$	2	2.09	2.13	2.13	1.96	1.78	
Mn^{III}SOD (1ix9)[22]		2.15	2.14	2.12	2.02	2.12	
second subunit		2.14	2.14	2.12	2.03	2.16	
$[Mn^{III}(Im)_3(Ac)(H_2O_2)]^{2+}$	2	2.02	2.03	2.05	1.95,2.21		2.40,3.16
$[Mn^{III}(Im)_3(AcH)(OH)(H_2O_2)]^{2+}$	2	2.07	2.03	2.04	2.18	1.90	2.43,3.19
$[Mn^{III}(Im)_3(Ac)(OH)(H_2O_2)]^+$	2	2.06	2.04	2.04	2.10	1.83	2.52,3.43
$[Mn^{III}(Im)_3(AcH)(OH)]^{2+}+H_2O_2$	2	2.07	2.05	2.04	2.08	1.83	4.29
$[Mn^{III}(Im)_3(Ac)(OH)]^+ + H_2O_2$	2	2.09	2.12	2.15	1.95	1.80	4.13
$[Mn(Im)_3(Ac)(O_2)]^+$	3/2	2.19	2.12	2.14	2.01,2.30		1.88,2.78
$[Mn(Im)_3(Ac)(H_2O)(O_2)]^+$	3/2	2.21	2.18	2.18	1.98	2.23	1.91,2.80
$Mn(Im)_3(Ac)(OH)(O_2)$	3/2	2.43	2.21	2.16	2.18	1.83	1.92,2.74
$[Mn(Im)_3(Ac)(H_2O)+O_2]^+$	7/2	2.25	2.18	2.19	2.05	2.21	5.09
$[Mn(Im)_3(Ac)(OH)+O_2]^0$	7/2	2.32	2.33	2.35	2.27,2.30	2.05	4.14
$[Mn(Im)_3(Ac)(HO_2)]^{2+}$	3/2	2.02	1.99	1.99	1.98,1.98		1.83,2.81
$[Mn(Im)_3(AcH)(OH)(HO_2)]^{2+}$	3/2	2.05	2.03	2.03	2.01	1.83	1.83,2.74
$[Mn(Im)_3(Ac)(OH)(HO_2)]^+$	3/2	2.06	2.08	2.07	1.99	1.79	2.14,3.11
$[Mn(Im)_3(AcH)(OH)+HO_2]^{2+}$	5/2	2.07	2.04	2.05	2.07	1.83	4.07
$[Mn(Im)_3(Ac)(OH)+HO_2]^+$	5/2	2.14	2.08	2.11	1.95	1.81	4.14
$Mn(Im)_3(Ac)(O_2)$	2	2.16	2.20	2.23	2.14,2.35		1.85,2.83
$Mn(Im)_3(Ac)(H_2O)(O_2)$	3	2.28	2.34	2.35	2.14	2.19	2.19,2.97
$[Mn(Im)_3(Ac)(OH)(O_2)]^-$	3	2.27	2.45	2.49	2.36	2.02	2.19,3.19
$[Mn(Im)_3(Ac)(H_2O)+O_2]^0$	3	2.33	2.21	2.20	2.08	2.06	4.24
$[Mn(Im)_3(Ac)(OH)+O_2]^-$	3	2.37	2.20	2.21	2.24	1.95	4.34
$[Mn(Im)_3(Ac)(HO_2)]^+$	2	2.21	2.10	2.12	2.00,2.42		1.85,2.75
$[Mn(Im)_3(Ac)(H_2O)(HO_2)]^+$	2	2.22	2.16	2.17	1.96	2.23	1.85,2.71
$Mn(Im)_3(Ac)(OH)(HO_2)$	2	2.11	2.33	2.37	2.01	1.85	2.07,3.09
$[Mn(Im)_3(Ac)(H_2O)+HO_2]^+$	3	2.25	2.18	2.20	2.05	2.20	4.41
$[Mn(Im)_3(Ac)(OH)+HO_2]^0$	3	2.37	2.20	2.25	2.07	2.03	4.28

Table 5. Binding energies (in kJ/mole) of water and OH^- to various complexes. The latter have been calculated from the binding of H_2O, followed by its deprotonation by Im.

#	Complex	Fe				Mn			
		ΔE	ΔG			ΔE	ΔG		
		ε = 1	ε = 1	ε = 4	ε = 80	ε = 1	ε = 1	ε = 4	ε = 80
	Binding of H_2O								
1	$[M^{II}(Im)_3(Ac)]^+$	5	24	**17**	13	3	20	**12**	7
2	$[M^{III}(Im)_3(Ac)]^{2+}$	-13	9	**11**	12	-37	-15	**-15**	-16
3	$[M^{III}(Im)_3(Ac)(H_2O_2)]^{2+}$	-14	15	**12**	11	-30	0	**-2**	-3
4	$M(Im)_3(Ac)(O_2)$	0	20	**20**	19	-18	-7	**-7**	-6
5	$[M(Im)_3(Ac)(O_2)]^+$	-41	-7	**-11**	-12	-16	8	**8**	8
6	$[M(Im)_3(Ac)(HO_2)]^+$	2	10	**10**	12	-15	5	**5**	6
7	$[M(Im)_3(Ac)(HO_2)]^{2+}$	-32	-10	**-5**	-3	-34	-16	**-13**	-11
	Binding of OH^-								
8	$[M^{II}(Im)_3(Ac)]^+$	8	23	**86**	110	1	22	**83**	106
9	$[M^{III}(Im)_3(Ac)]^{2+}$	-459	-431	**-155**	-27	-481	-451	**-176**	-49
10	$[M^{III}(Im)_3(Ac)(H_2O_2)]^{2+}$	-468	-443	**-173**	-47	-453	-435	**-164**	-38
11	$M(Im)_3(Ac)(O_2)$	334	343	**197**	118	359	361	**224**	153
12	$[M(Im)_3(Ac)(O_2)]^+$	-70	-45	**16**	39	-68	-49	**15**	40
13	$[M(Im)_3(Ac)(HO_2)]^+$	24	47	**110**	134	16	36	**100**	125
14	$[M(Im)_3(Ac)(HO_2)]^{2+}$	-450	-424	**-152**	-25	-396	-374	**-106**	18

Table 6. Deprotonation energies of various complexes, compared to the deprotonation energy of ImH^+, i.e. the energy (in kJ/mole) of the reaction $X(H_2O) + Im \rightarrow X(OH^-) + ImH^+$ with various complexes *X*.

		Fe				Mn			
		ΔE	ΔG			ΔE	ΔG		
#	*X*	ε = 1	ε = 1	ε = 4	ε = 80	ε = 1	ε = 1	ε = 4	ε = 80
1	$[M^{II}(Im)_3(Ac)]^+$	2	0	**70**	97	-2	2	**71**	99
2	$[M^{III}(Im)_3(Ac)]^{2+}$	-447	-440	**-166**	-38	-443	-436	**-160**	-32
3	$[M^{III}(Im)_3(Ac)(H_2O_2)]^+$	-454	-458	**-185**	-58	-423	-435	**-162**	-35
4	$[M^{III}(Im)_3(Ac)]^{2+}+H_2O_2$	-434	-419	**-157**	-35	-427	-413	**-155**	-35
5	$[M(Im)_3(Ac)(O_2)]^+$	-30	-38	**26**	51	-52	-57	**7**	32
6	$[M(Im)_3(Ac)+O_2]^+$	-15	-15	**46**	69	-5	-3	**64**	92
7	$[M(Im)_3(Ac)(HO_2)]^{2+}$	-419	-413	**-146**	-22	-363	-358	**-93**	29
8	$[M(Im)_3(Ac)+HO_2]^{2+}$					-436	-431	**-173**	-54
9	$M(Im)_3(Ac)(O_2)$	334	323	**177**	99	377	368	**231**	159
10	$M(Im)_3(Ac)+O_2$	308	302	**168**	97	323	321	**188**	118
11	$[M(Im)_3(Ac)(HO_2)]^+$	22	38	**99**	122	31	31	**95**	119
12	$[M(Im)_3(Ac)+HO_2]^+$					-87	-76	**-8**	-55

Table 7. Reaction energies (ΔG in a protein-like continuum solvent with $\varepsilon = 4$; kJ/mole) of the relevant reactions. Note that the reactions involving H^+ actually have been calculated with the ImH^+/Im pair. The invariant $[(Im)_3(Ac)]^-$ ligands have also been omitted from both sides of all reactions.

#	Reaction	Dissoc.		Associative				Second-sphere			
				H_2O		OH^-		H_2O		OH^-	
		Fe	Mn	Fe	Mn	Fe	Mn	Fe	Mn	Fe	Mn
1	$M^{II} + {}^3O_2 \rightarrow [M(O_2)]^{2+}$	55	44	27	40	-16	-24	33	4	9	-4
2	$M^{II} + O_2^- \rightarrow [M(O_2)]^+$	-1	8	2	-11	110	149	-2	-4	96	113
3	$M^{III} + O_2^- \rightarrow [M(O_2)]^{2+}$	-215	-243	-237	-220	-45	-52	-231	-256	-19	-32
4	$M^{II} + HO_2 \rightarrow [M(HO_2)]^{2+}$	-40	-26	-46	-33	-16	-9	-6[b]	4	-48	-75
5	$M^{III} + HO_2 \rightarrow [M(HO_2)]^{3+}$	17	0	1	3	20	71	-6	6	-71[a]	-6
6	$M^{III} + HO_2^- \rightarrow [M(HO_2)]^{2+}$	-264	-268	-264	-247	1	8	-[c]	-210	-31	-57
7	$M^{III} + H_2O_2 \rightarrow M^{III}(H_2O_2)$	25	5	26	19	7	17	-2	3	7	9
8	$[M(O_2)]^+ + H^+ \rightarrow [M(HO_2)]^{2+}$	-32	-28	-42	-15	-120	-152	2[b]	14	-138	-181
9	$[M(O_2)]^{2+} + H^+ \rightarrow [M(HO_2)]^{3+}$	239	250	244	229	72	129	231	269	-46[a]	32
10	$[M(HO_2)]^{2+} + H^+ \rightarrow [M(H_2O_2)]^{3+}$	223	207	225	200	-59	-57	-[c]	148	-28	0
11	$[M(OH)(HO_2)]^{2+} \rightarrow [M(H_2O)(O_2)]^{+2}$					-98	-136			-[a]	-96
12	$[M(H_2O)(HO_2)]^{2+} \rightarrow [M(OH)(H_2O_2)]^{2+}$			40	38			-6/2[b]	-7		
13	$[M(H_2O)(O_2)]^+ \rightarrow [M(OH)(HO_2)]^+$			57	80			30	7		
14	$M^{II} \rightarrow M^{III} + e^-$ (eV)	2.36	2.54	2.30	2.26	-0.14	-0.14	2.30	2.26	-0.14	-0.14
15	$M^{II}(H_2O) \rightarrow M^{III}(OH) + H^+ + e^-$ (eV)			0.58	0.59			0.58	0.59		

[a] For this complex, reactions 5 and 11 are spontaneously followed by reaction 12 with a total barrier of –71 and –46 kJ/mole, respectively (the $[Fe(Im)_3(Ac)(H_2O)+(HO_2)]^+$ complex is unstable).

[b] For this complex, reactions 4 and 8 are spontaneously followed by reaction 12 with a total barrier of –6 and 2 kJ/mole, respectively (the $[Fe(H_2O)+(HO_2)]^{2+}$ complex is unstable).

[c] The $Fe(H_2O)+(HO_2)]^{2+}$ complex is unstable.

Figure 1. Optimised structures of some of the models: a) $[Fe^{III}(Im)_3(AcH)(OH)]^{2+}$; b) $[Fe^{III}(Im)_3(AcH)(OH)]^{2+}+H_2O_2$; c) $[Fe(Im)_3(Ac)(H_2O)(O_2)]^{+}$, with O_2 binding side-on; d) $[Fe(Im)_3(Ac)(HO_2)]^{2+}$, with Ac bidentate; e) $[Fe(Im)_3(Ac)(OH)(O_2)]^{-}$, with O_2 binding end-on; f) $Fe(Im)_3(Ac)(OH)+(HO_2)$.

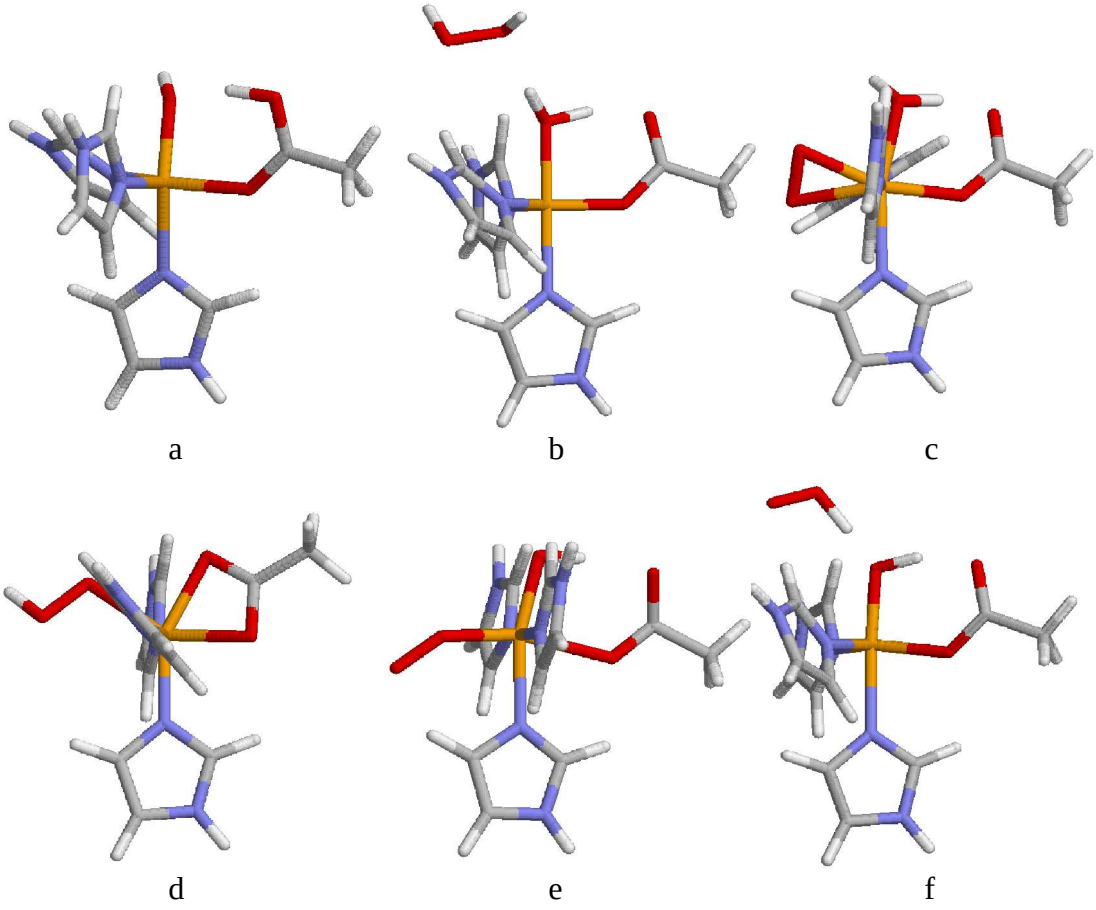

Figure 2. The suggested reaction mechanisms for the two half-reactions of FeSOD. The numbers above the arrows are the estimated ΔG of the reactions (in kJ/mole at ε = 4 and pH 7.0).

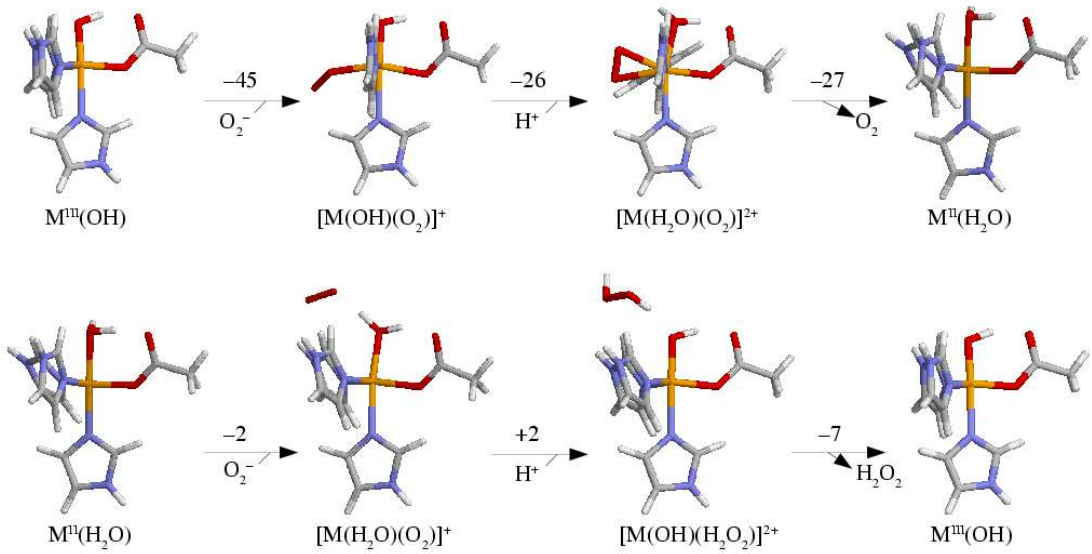

[1] Fridovich I. Annu. Rev. Biochem. 1995, 64, 97-112.
[2] Stallings W. C.; Pattridge K. A.; Strong R. K.; Ludwig M. L. J. Biol. Chem. 1984, 259, 10695-10699.
[3] Miller A.-F. In Handbook of Metalloproteins, Messerschmidt A.; Huber R.; Wieghardt K.; Poulos T., Eds, John Wiley & Sons: Chichester 2001, pp 668-692.
[4] Stroupe M. E.; DiDonato M.; Tainer J. A. In Handbook of Metalloproteins, Messerschmidt A.; Huber R.; Wieghardt K.; Poulos T. Eds, John Wiley & Sons: Chichester 2001, pp 941-951.
[5] Bordo D.; Pesce A.; Bolognesi M.; Stroppolo M. E.; Falconi M.; Desideri A. In Handbook of Metalloproteins, Messerschmidt A.; Huber R.; Wieghardt K.; Poulos T., Eds, John Wiley & Sons: Chichester 2001, pp 1284-1300.
[6] Lee J.-W.; Roe J.-H.; Kang S.-O. Meth. Enzym. 2002, 349, 90-101.
[7] Wuerges J.; Lee J.-W.; Yim Y.-I.; Yim H.-S.; Kang S.-O.; Carugo K. D. Proc. Natnl. Acad. Sci. USA 2004, 101, 8569-8574.
[8] Barondeau D. P.; Kassmann C. J.; Bruns C. K.; Tainer J. A.; Getzoff E. D. Biochemistry 2004, 43, 8038-8047.
[9] Ullah Khan A.; Kasha M. Proc. Natnl. Acad. Sci. USA 1994, 91, 12365-12367.
[10] Miller A.-F.; Sorkin. D. L. Comments Mol. Cell Biophys. 1997, 9, 1-48.
[11] Getzoff E. D.; Tainer J. A.; Stempien M. M.; Bell G. I.; Hallewell R. A. Proteins Struct. Funct. Genet. 1989, 5, 322-336.
[12] Hassan H. M.; Fridovich I. Eur. J. Rheumatol. Inflamm. 1981, 4, 160-172.
[13] Steinman H. M.; Weinstein L.; Brenowitz M. J. Biol. Chem. 1994, 269, 28629-28634.
[14] Chance B.; Sies H.; Boveris A. Physiol. Rev. 1979, 59, 527-605.
[15] Hopkin K. A.; Papazian M. A.; Steinman H. M. J. Biol. Chem. 1992, 267, 24253-24258.
[16] Bull C.; Niederhoffer E. C.; Yoshida T.; Fee J. A. J. Am. Chem. Soc. 1991, 113, 4069-4076.
[17] Riley D. P. Chem. Rev. 1999, 99, 2573-2587.
[18] Sayre L. M.; Perry G.; Smith M. A. Curr. Opin. Chem. Biol. 1999, 3, 220-225.
[19] McCord J. M. Meth. Enzym. 2002, 349, 331-341.
[20] Hsu J. L.; Hsieh Y.; Tu C.; O'Connor D.; Nick H. S.; Silverman A. N. J. Biol. Chem. 1996, 271, 17687-17691.
[21] Vance C. K.; Miller A.-F. J. Am. Chem. Soc. 11998, 20, 461-467.
[22] Anderson B. F.; Edwards R. A.; Whittaker M. M.; Whittaker J. W.; Baker E. N.; Jameson G. B., to be published, PDB files 1ix9 and 1ixb
[23] Lah M. S.; Dixon M. M.; Pattridge K. A.; Stallings W. C.; Fee J. A.; Ludwig M. L. Biochemistry 1995, 34, 1646-1660.
[24] Kerfeld C. A.; Yoshida S.; Tran K. T.; Yeates T. O.; Cascio D.; Bottin H.; Berthomieu C.; Sugiura M.; Boussac A. J. Biol. Inorg. Chem. 2003, 8, 707-717.
[25] Stallings W. C.; Metzger A. L.; Pattridge K. A.; Fee J. A.; Ludwig M. L. Free Rad. Res. Commun. 1991,12-13, 259-268.
[26] Han W.-G.; Lovell T.; Noodleman L. Inorg. Chem. 2002, 41, 205-218.
[27] Hunter T.; Ikebukuro K.; Bannister W. H.; Bannister J. V.; Hunter G. J. Biochemistry 1997, 36, 4925-4933.
[28] Jackson T. A.; Brunold T. C. Acc. Chem. Res. 2004, 37, 461-470.
[29] Hsieh Y.; Guan Y.; Tu C.; Bratt P. J.; Angerhofer A.; Lepock J. R.; Hickey M. J.; Tainer J. A.; Nick H. S.; Silverman D. N. Biochemistry 1998, 37, 4731-4739.
[30] Yikilmaz E.; Xie J.; Brunold T. C.; Miller A.-F. J. Am. Chem. Soc. 2002, 124,

3482-3483.
[31] Miller A.-F.; Padmakumar K.; Sorkin D. L.; Karapetian A.; Vance C. K. J. Inorg. Biochem. 2003, 93, 71-83.
[32] Lah M. S.; M. M Dixon.; Pattridge K. A.; Stallings W. C.; Fee J. A.; Ludwig M. L. Biochemistry 1995, 34, 1646-1660.
[33] Jackson T. A.; Yikilmaz E.; Miller A.-F.; Brunold T. C. J. Am. Chem. Soc. 2003, 125, 8348-8363.
[34] Whittaker J. W.; Whittaker M. M. J. Am. Chem. Soc. 1991, 113, 5528-5540.
[35] Whittaker J. W.; Solomon E. I. J. Am. Chem. Soc. 1988, 110, 5329-5339.
[36] Vatyam S.; Byrd R. A.; Miller A.-F. Magn. Reson. Chem. 2000, 38, 536-542.
[37] Miller A.-F.; Sorkin D. L.; Padmakumar K. Biochemistry 2005, 44, 5969-5981.
[38] Whittaker M. M.; Whittaker J. W. Biochemistry 1996, 35, 6762-6770.
[39] Whittaker M. M.; Whittaker J. W. J. Biol. Inorg. Chem. 1997, 2, 667-671.
[40] Jackson T. A.; Karapetian A.; Miller A.-F.; Brunold T. C. J. Am. Chem. Soc. 2004, 126, 12477-12491.
[41] Sines J.; Alison S; Wierzbicki A.; McCammon J. A. J. Phys. Chem. 1990, 94, 959-961.
[42] Whittaker M. M.; Ekberg C. A.; Edwards R. A.; Baker E. N.; Jameson G. B.; Whittaker J. W. J. Phys. Chem. B 1998, 102, 4668-4677.
[43] Yikilmaz, E.; Xie J.; Brunold T. C.; Miller A.-F. J. Am. Chem. Soc. 2002, 124, 3482-3483.
[44] Xie J.; Yikilmaz E.; Miller A.-F.; Brunold T. C. J. Am. Chem. Soc. 2002, 124, 3769-3774.
[45] Jackson T. A.; Xie, J.; Yikilmaz E.; Miller A.-F.; Brunold T. C. J. Am. Chem. Soc. 2002, 124, 10833-10845.
[46] Fisher C. L.; Chen J.-L.; Li J.; Bashford D.; Noodleman L. J. Phys. Chem. 11996, 00, 13498-13505.
[47] Li J.; Fisher C. L.; Konecny R.; Bashford D.; Noodleman L. Inorg. Chem. 1999, 38, 929-939.
[48] Treutler O.; Ahlrichs R. J. Chem. Phys. 1995, 102, 346-354.
[49] Becke A. D. Phys. Rev. A 1988, 38, 3098-3100.
[50] Perdew J. P. Phys. Rev. B 1986, 33, 8822-8824.
[51] Schäfer A.; Horn H.; Ahlrichs, R. J. Chem. Phys. 1992, 97, 2571-2577.
[52] Schäfer A.; Huber C.; Ahlrichs, R. J. Chem. Phys. 1994, 100, 5829-5835.
[53] Hehre W. J.; Radom L.; Schleyer P. v. R.; Pople J. A. 1986, In Ab initio molecular orbital theory, Wiley-Interscience, New York.
[54] Eichkorn K.; Treutler O.; Öhm H.; Häser M.; Ahlrichs R. Chem. Phys. Lett. 1995, 240, 283-290.
[55] Eichkorn K.; Weigend F.; Treutler O.; Ahlrichs R. Theor. Chem. Acc. 1997, 97, 119-124.
[56] Hertwig R. H .; Koch W. Chem. Phys. Lett. 1997, 268, 345-351.
[57] Jensen F. Introduction to Computational Chemistry John Wiley & Sons, 1999.
[58] Amzel L. M. Proteins Struct Funct Gen 1997, 28, 144-149.
[59] Bauschlicher C. W. Chem. Phys. Lett. 1995, 246, 40-44.
[60] Curtiss L. A.; Raghavachari K.; Redfern P. C.; Pople J. A. J. Chem. Phys. 1997, 106, 1063-1079.
[61] Curtiss L. A.; Raghavachari K.; Redfern P. C.; Pople J. A. J. Chem. Phys. 2000, 112, 7374-7383.
[62] Siegbahn P. E. M.; Blomberg M. R. A Annu. Rev. Phys. Chem. 1999, 50 221–249.

[63] Siegbahn P. E. M.; Blomberg M. R. A. Chem. Rev. 2000, 100, 421–437.
[64] Peterson J.; Fee J. A.; Day E. P. Biochim. Biophys. Acta 1991, 113, 5528-5540.
[65] Klamt A.; Schuurmann G. J. Chem. Soc. Perkin Trans. 2 1993, 799-805.
[66] Schäfer A.; Klamt A.; Sattel D.; Lohrenz J. C. W.; Eckert F. PhysChemChemPhys 2000, 2, 2187-2193.
[67] Sharp K. A. Annu. Rev. Biophys. Biophys. Chem. 1990, 19, 301-332.
[68] Honig B. Science 1995, 268, 1144-1149.
[69] Klamt A.; Jonas V.; Bürger T.; Lohrenz J. C. W. J. Phys. Chem. 1998, 102, 5074-5085.
[70] Reiss H.; Heller A. J. Phys. Chem. 1985, 89, 4207-4213.
[71] Scheidt W. R.; Reedk C. A. Chem. Rev. 1981, 81, 543-555.
[72] Siegbahn P. E. M. Curr. Opin. Chem. Biol. 2002, 6, 227-235.
[73] Sigfridsson E.; Olsson M. H. M.; Ryde U. J. Phys. Chem. B 2001, 105, 5546-5552.
[74] Olsson M. H. M.; Ryde U. J. Am. Chem. Soc. 2001, 123, 7866-7876.
[75] Ryde U.; Nilsson K. J. Am. Chem. Soc. 2003, 125, 14232-14233.
[76] Wilmot C. M.; Sjögren T.; Carlsson G. H.; Berglund G. I.; Hajdu, J. Methods Enzymol. 2002, 353, 301-318.
[77] Rulisek L.; Ryde U, submitted to J. Inorg. Biochem.
[78] Fields B. A.; Bartsch H. H.; Bartunik H. D.; Cordes F.; Guss J. M.; Freeman H. C. Acta Crystallogr. D 1994, 50, 709-730.
[79] Cruickshank D. W. J. Acta Crystallogr. D 1999, 55, 583-601.
[80] Nilsson K.; Lecerof D.; Sigfridsson E.; Ryde U. Acta Crystallogr. D 2003, 59, 274-289.
[81] Nilsson K.; Ryde U. J. Inorg. Biochem. 2004, 98, 1539-1546.
[82] Holm R. H.; Kennepohl P.; Solomon E. I. Chem. Rev. 1996, 96, 2239-2314.
[83] Ryde U. Eur. J. Biophys. 1996, 24, 213-221.
[84] Noodleman L.; Lovell T .; Han W.-G .; Li J.; Himo F. Chem. Rev. 2004, 104, 459-508.
[85] Pelmenschikov V.; Siegbahn P. E. M. Inorg. Chem. 2005, 44, 3311-3320.
[86] Jensen K. P.; Ryde U. J. Biol. Chem. 2004, 279, 14561-14569.
[87] Danovich D.; Shaik S. J. Am. Chem. Soc. 1997, 119, 1773-1786.